A role for the spinal cord cholinergic neuron circadian clock in RNA metabolism and mediating ALS disease phenotypes

Sharon B. Tam[1], Nathan J. Waldeck[2], Matthew Wright[1,3], Jelena Mojsilovic-Petrovic[1], Erin M. Baker[1], Evangelos Kiskinis[1,3], Joseph Bass[2], Robert G. Kalb[1*]

[1]The Ken & Ruth Davee Department of Neurology, Northwestern University Feinberg School of Medicine, Chicago, IL 60611, USA.

[2]Department of Medicine, Division of Endocrinology, Metabolism, and Molecular Medicine, Northwestern University Feinberg School of Medicine, Chicago, IL 60611, USA.

[3]Department of Neuroscience, Northwestern University Feinberg School of Medicine, Chicago, IL 60611, USA.

*Correspondence: robert.kalb1@northwestern.edu

Keywords: alternative splicing, amyotrophic lateral sclerosis (ALS), circadian clock, neurodegeneration, RNA-binding protein (RBP), RNA metabolism, spinal cord cholinergic neuron, transcriptomics

ABSTRACT

Circadian clocks are encoded by a transcription-translation feedback loop that aligns physiological processes with the solar cycle. Previous work linking the circadian clock to the regulation of RNA-binding proteins (RBPs) and alternative splicing provides a foundation for the vital examination of their mechanistic connections in the context of amyotrophic lateral sclerosis (ALS)—a fatal neurodegenerative disease commonly marked by disrupted RBP function. Here, we reveal that the spinal cord cholinergic neuron rhythmic transcriptome is enriched for genes associated with ALS and other neurodegenerative diseases. We show that there is time-of-day-dependent expression of ALS-linked RBP transcripts and rhythmic alternative splicing of genes involved in fundamental neuronal processes, such as microtubule cytoskeleton organization, intracellular trafficking, and synaptic function. We demonstrate clock-dependent expression of ALS-linked RBP Ataxin 2 in this neuronal subtype. Further, through *in silico* analysis of RNA sequencing data from sporadic ALS patients, we find that gene expression profiles altered in disease correspond with rhythmic gene networks. Finally, we report that clock disruption through cholinergic neuron-specific deletion of clock activator BMAL1 (*i*) increases lumbar spinal cord motor neuron loss and sciatic nerve axon degeneration and (*ii*) drives time-of-day-dependent alternative splicing of genes associated with RNA metabolism, including genes encoding ALS-linked RBPs (e.g., *Matr3*, *Srsf7*, and *Ythdf2*). Our results establish a role for the cholinergic neuron circadian clock in RNA metabolism and mediating neurodegeneration.

INTRODUCTION

The circadian system acts as a biological timekeeper that aligns physiological energetic cycles with the day/night cycle. In mammals, the molecular clock is encoded by a transcription-translation feedback loop comprised of activators (CLOCK and BMAL1) that induce the transcription of repressors (PERs and CRYs), which feedback to inhibit the forward limb in a cycle that repeats itself every ~24 hours, with a stabilizing loop consisting of REV-ERB and ROR transcription factors that modulate BMAL1 expression (Bass 2012). In recent decades, clock transcriptional regulation has been characterized in diverse mammalian tissues and is estimated to drive the rhythmic expression of 10-15% of all mRNAs within a given tissue (Lowrey and Takahashi 2004; Panda et al. 2002; Vollmers et al. 2009). Intriguingly, recent studies in liver have demonstrated that most of the genes that exhibit rhythmic mRNA expression do not exhibit rhythmic expression of the corresponding intron-containing pre-mRNA, suggesting that post-transcriptional modifications play a major role in the regulation of circadian gene expression (Green 2018; Koike et al. 2012; Kojima et al. 2011; Menet et al. 2012).

Emerging evidence points to a connection between the circadian clock and RNA-processing events, such as methylation, polyadenylation, and alternative splicing (Fustin et al. 2013; Kojima et al. 2012; Marcheva et al. 2020). Time-of-day-dependent production of alternatively spliced transcripts has been previously reported in plants, flies, and mice, primarily in neuronal cell-types (Hughes et al. 2012; Marcheva et al. 2020; McGlincy et al. 2012; Sanchez et al. 2010; Wang et al. 2018; Yang et al. 2020). Alternative splicing allows a single gene to produce multiple distinct mRNA transcripts in a tissue- and cell-type specific manner, which contributes to transcriptomic diversity and enables cells to perform complex and specialized functions (Chen and Manley 2009; Young et al. 1981). This process is strongly regulated by RNA-binding proteins (RBPs), which bind to specific regulatory sequence motifs in pre-mRNA and either enhance or suppress spliceosome recruitment to splice sites (Ule and Blencowe 2019). While RBPs are ubiquitously expressed, cells and tissue within the central nervous system (CNS) demonstrate greater disease vulnerability to RBP dysregulation due to their higher frequency of alternative splicing (Pan et al. 2008; Yeo et al. 2004).

Disrupted RBP homeostasis is a hallmark of many neurological diseases, including amyotrophic lateral sclerosis (ALS), which is a progressive neurodegenerative disease that originates in upper and lower motor neurons in the brain and spinal cord (Nussbacher et al. 2019; Prashad and Gopal 2021). Genetic studies have revealed associations between ALS and mutations in genes encoding a number of RBPs, including TDP-43, FUS, ATXN2, TAF15, EWSR1, hnRNPA1, hnRNPA2B1, MATR3, and TIA1 (Kapeli et al. 2017; Zhao et al. 2018). These RBPs are key regulators of RNA metabolism and neuronal health, and ALS-linked mutations have been shown to vastly disrupt RNA processes, such as alternative splicing, mRNA transport, liquid phase transitions, and local translation (Kapeli et al. 2017; Nagano and Araki 2021). For example, many of the proteins that co-purify with TDP-43 are associated with RNA splicing and translation (Freibaum et al. 2010), and ALS-linked mutations in TDP-43 were shown to impair mRNA axonal transport and alter the fluid properties of TDP-43-positive liquid droplets (Alami et al. 2014; Schmidt and Rohatgi 2016).

Previous work linking the circadian clock to RBP function provides a foundation for the critical examination of their mechanistic connections in the context of ALS (Marcheva et al. 2020; Wang et al. 2018). The role of the lower motor neuron (LMN) clock in disrupted RBP function and alternative splicing as it relates to ALS disease pathophysiology is not known. Here, we perform transcriptomic analysis of spinal cord cholinergic neurons to elucidate the time-of-day-dependent effects of cell-type-specific clock disruption. We report that the cholinergic neuron rhythmic transcriptome is enriched for genes associated with ALS and other neurodegenerative diseases. We show that there is time-of-day-dependent expression of ALS-linked RBP transcripts and rhythmic alternative splicing of genes involved in microtubule cytoskeleton organization, intracellular trafficking, and synaptic function. In addition, we demonstrate clock-dependent expression of ALS-linked RBP Ataxin 2 (ATXN2) in this neuronal subtype. Through *in silico* analysis of RNA sequencing (RNA-seq) data from sporadic ALS (sALS) patients, we find that gene expression profiles altered in disease correspond with rhythmic gene networks. Finally, we report that clock disruption through cholinergic neuron-specific deletion of clock activator BMAL1 (*i*) increases lumbar spinal cord motor neuron loss and sciatic nerve axon degeneration and (*ii*) drives time-of-day-dependent alternative splicing of genes associated with RNA processing, including genes

encoding ALS-linked RBPs (e.g., *Matr3*, *Srsf7*, and *Ythdf2*). Thus, we propose that disruption of the cholinergic neuron circadian clock alters RNA metabolism and contributes to ALS disease phenotypes.

RESULTS

Spinal cord cholinergic neuron rhythmic transcriptome is enriched for genes associated with ALS and other neurodegenerative diseases

Given that ALS disease fatality stems from cellular dysfunction occurring within acetylcholine-releasing LMNs, also known as spinal cord cholinergic neurons, we aimed to characterize the rhythmic transcriptome of this neuronal subtype. To elucidate the cholinergic neuron transcriptome, we first generated *ChAT-Cre*;*RiboTag*$^{fx/+}$ mice, which possess a ribosomal hemagglutinin (HA) tag to enable the isolation and characterization of mRNAs specifically bound to cholinergic neuron ribosomes. We harvested and isolated RNA from wild-type (WT) spinal cord cholinergic neurons every 4 h across the 24-hr day for RNA-seq (Fig. 1A and S1A-B). Rhythmic transcriptome profiling revealed 2,391 oscillating transcripts (~12% of genes) by Jonckheere-Terpstra-Kendall (JTK) Cycle analysis, with most rhythmic transcripts reaching maximal abundance at Zeitgeber Time (ZT) 20 and 22 in the dark/active period, and a smaller cluster of genes reaching peak expression at ZT8 in the light/rest period (Fig. 1B-C; Table S1A). Kyoto Encyclopedia of Genes and Genomes (KEGG) pathway analysis showed overall enrichment of genes associated with *(i)* neurodegenerative diseases (ALS, Parkinson's disease, Huntington's disease, prion disease, and spinocerebellar ataxia), *(ii)* protein synthesis and degradation (spliceosome, ribosome, protein processing in the endoplasmic reticulum, proteasome, and ubiquitin-mediated proteolysis), *(iii)* metabolism (oxidative phosphorylation, TCA cycle, and metabolic pathways), and *(iv)* synaptic transmission (GABAergic synapse, dopaminergic synapse, and long-term potentiation) (Fig. 1D).

Notably, we found significant enrichment of the oscillating transcripts for KEGG pathway genes associated with ALS, including genes related to oxidative phosphorylation, autophagy, and the oxidative stress response (Fig. 1E; Table S1B). In addition, 15 of the rhythmically expressed ALS genes were associated with the Gene Ontology (GO) term "cytoskeleton organization," including *Pfn1*, *Dctn2*, and *Nefm* (Fig. 1F; Table S1B). In analyzing the genes with peak expression during the light and dark periods

separately, we found 711 rhythmic genes with peak abundance during the light period (ZT0-12), and GO enrichment analysis revealed over-representation for RNA processing (e.g., mRNA splicing) and biosynthetic processes (e.g., translation) (Fig. S2). In contrast, 1,680 rhythmic genes exhibited peak abundance during the dark period (ZT12-24), and GO analysis revealed enrichment for pathways associated with protein localization and transport (Fig. S2). Our findings suggest that these processes are regulated by the circadian clock in cholinergic neurons.

Figure 1

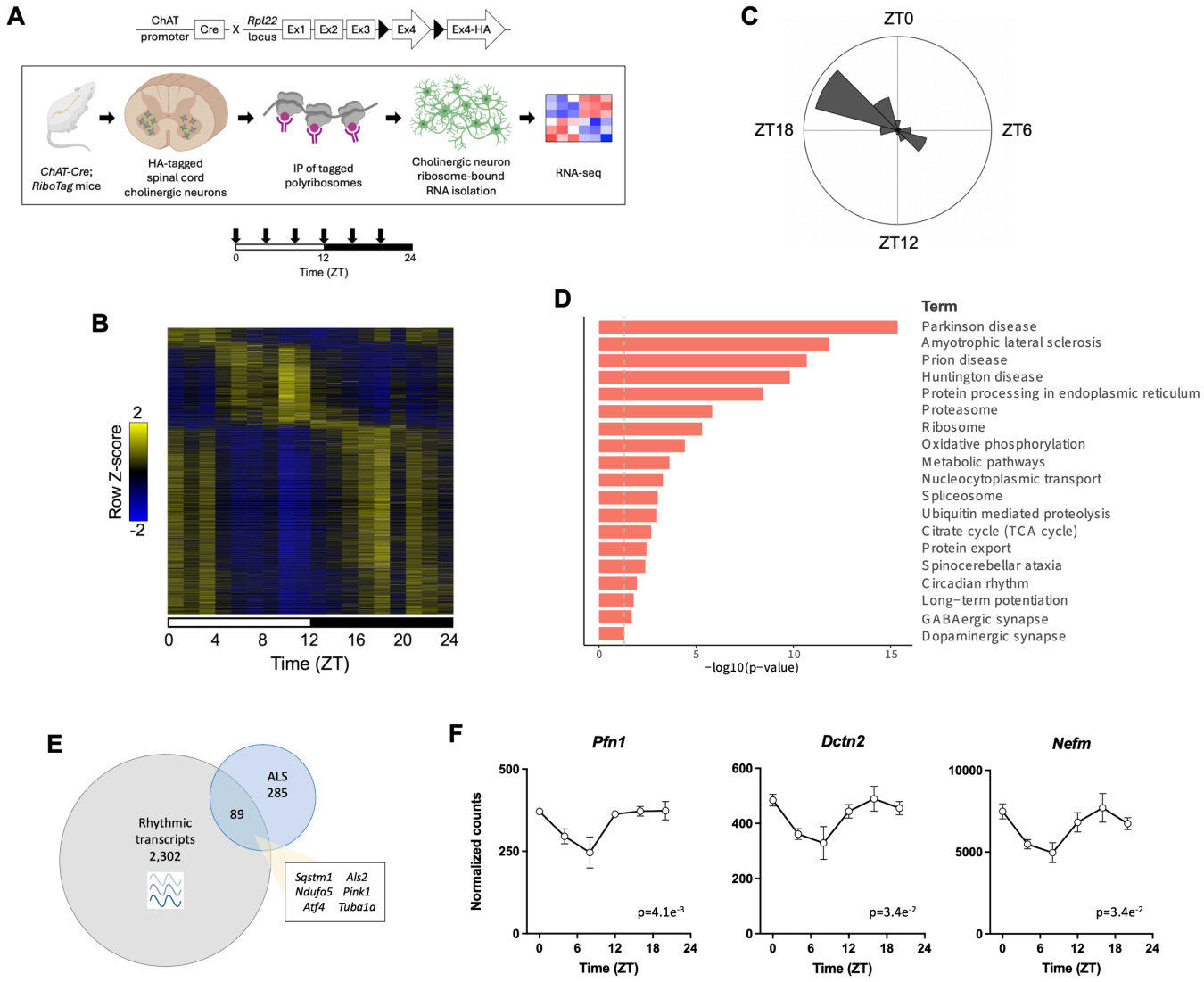

Figure 1. Spinal cord cholinergic neuron rhythmic transcriptome is enriched for genes associated with ALS and other neurodegenerative diseases. (A) Schematic showing RNA isolation in wild-type (WT) spinal cord cholinergic neurons from 10-week-old *ChAT-Cre*;*RiboTag*$^{fx/+}$ male mice collected every 4 h across the 24-hr day for RNA-seq. Down arrows indicate sample harvesting times (ZT0, 4, 8, 12, 16, and 20). Created using BioRender. **(B)** Heatmap showing rhythmic cholinergic neuron mRNA expression (n = 3 per time point). **(C)** Radial histogram showing the number of oscillating genes that have peak expression within each 2-hr window. **(D)** KEGG pathway analysis of all oscillating genes in cholinergic neurons. **(E)** Enrichment of KEGG pathway ALS genes among rhythmic transcripts in WT cholinergic neurons (adjusted $p < 0.0001$ in hypergeometric test). **(F)** Examples of time-of-day-dependent expression of ALS-linked genes that regulate cytoskeleton dynamics, shown as normalized counts identified through DESeq2 (n = 3 per time point). Data are represented as mean ± SEM. Rhythmicity was determined by JTK_Cycle analysis (adjusted p-value shown).

Circadian clock regulates expression of ALS-linked RBPs and alternative splicing in spinal cord cholinergic neurons

RNA-binding proteins regulate alternative splicing by interacting with regulatory elements in pre-mRNA to guide spliceosome recruitment (Ule and Blencowe 2019). Clues to the rhythmic expression of genes encoding ALS-linked RBPs in neuronal subtypes originated from earlier studies demonstrating oscillatory RBP abundance in various mouse CNS regions, including brain stem, suprachiasmatic nucleus (SCN), hypothalamus, and pituitary (Fig. S3) (Pizarro et al. 2013). To determine whether RBP-mediated alternative splicing is regulated by the circadian clock in cholinergic neurons, we assessed rhythmic RBP expression and identified 70 oscillating transcripts that encode splicing-related RBPs, including 5 that overlap with rhythmically expressed ALS genes—*Fus*, *Hnrnpa2b1*, *Atxn2*, *Taf15*, and *Ncbp1* (Fig. 2A; Table S1C). Based on these findings, we proposed that there is clock regulation of ALS-linked RBP expression and alternative splicing in this neuronal subtype. To test this hypothesis, we first analyzed RBP protein expression in primary rat spinal cord cholinergic neurons with siRNA knockdown of *Bmal1* and scramble (SCR) controls. Notably, we found a significant decrease in Ataxin2 (ATXN2) with *Bmal1*-loss (Fig. 2B), which suggests that ATXN2 protein expression is clock-dependent. Given that we did not observe differential mRNA expression of *Atxn2* (or other rhythmically expressed ALS-linked RBP transcripts) with cholinergic neuron-specific *Bmal1*-deletion, it is likely that this decrease in ATXN2 expression is a result of clock-driven post-translational events. In key studies performed in *Drosophila*, the ATXN2 homolog has been found to contribute to the regulation of circadian rhythms by activating the translation of core clock protein PERIOD (PER) (Lim and Allada 2013; Zhang et al. 2013). Further, a recent report demonstrated ATXN2 regulation of PER2 translation and oscillatory phase separation in mouse SCN (Zhuang et al. 2023).

We observed a bimodal distribution in peak phases of mRNA abundance of the oscillating splicing-associated RBPs 12 hours apart at ZT8 and ZT20 (Fig. 2C). To next determine whether alternative pre-mRNA splicing in cholinergic neurons is influenced by circadian time, we used replicate multivariate analysis of transcript splicing (rMATS) to identify alternative splicing events in WT cholinergic neurons collected at 4-hr intervals (Fig. 1A), including skipped exons (SE), mutually exclusive exons

(MXE), and alternative 3' and 5' splice sites (A3SS and A5SS). We calculated the percent-spliced in (psi, Ψ) value for all common alternative splicing events in each of the three replicate samples at each time point and performed JTK_Cycle analysis to identify statistically significant oscillations in Ψ. This analysis revealed 11 rhythmic alternative splicing events, consisting of 8 SE, 1 MXE, 1 A3SS, and 1 A5SS (Fig. 2D; Table S2A-D). Peak Ψ values also displayed a bimodal distribution 12 hours apart (at ZT0-2 and ZT12-14), with most Ψ values peaking at ZT12 (Fig. 2E). Sashimi plots, which illustrate exon inclusion levels by mapping reads across splice junctions, are shown throughout the circadian day to demonstrate rhythmic splicing of representative gene *Aftph*, which encodes Aftiphilin—a factor that enables clathrin binding and intracellular transport as part of the AP-1 adaptor complex (Fig. 2F) (Burman et al. 2005). We found that *Aftph* was rhythmically spliced by both SE and A5SS (Fig. 2D; Tables S2A and S2D).

LIMCH1 promotes actin stress fiber assembly and focal adhesion, and alternative splicing of *Limch1* is associated with muscle weakness and calcium-handling deficits (Lin et al. 2017; Penna et al. 2023). Our data revealed that both *Limch1* and dynein regulatory complex gene *Drc3* are rhythmically alternatively spliced by SE (Fig. 2D; Table S2A). In addition, Rap GTPase-activating protein (RapGAP) encoding gene *Sipa1l2* regulates synaptic function and vesicle trafficking at presynaptic terminals, and we found that it also displayed rhythmic altered splicing by SE (Fig. 2D; Table S2A) (Andres-Alonso et al. 2019). Two genes exhibited both rhythmic mRNA expression and rhythmic splicing: vesicle trafficking gene *Mvb12a* and apoptosis gene *Pdcd2l* (Fig. 2G) (Gao et al. 2022; Tsunematsu et al. 2010). We establish here that genes involved in microtubule cytoskeleton organization, intracellular trafficking, and synaptic function are rhythmically spliced in cholinergic neurons. Of note, a previous report demonstrated that rhythmically spliced genes in pancreatic islets were similarly associated with trafficking, exocytosis, and synaptic regulation (Marcheva et al. 2020). Taken together, these data demonstrate time-of-day-dependent expression of ALS-linked RBP transcripts as well as clock-dependent expression of ATXN2, and establish for the first time that the circadian clock regulates alternative splicing in cholinergic neurons.

Figure 2

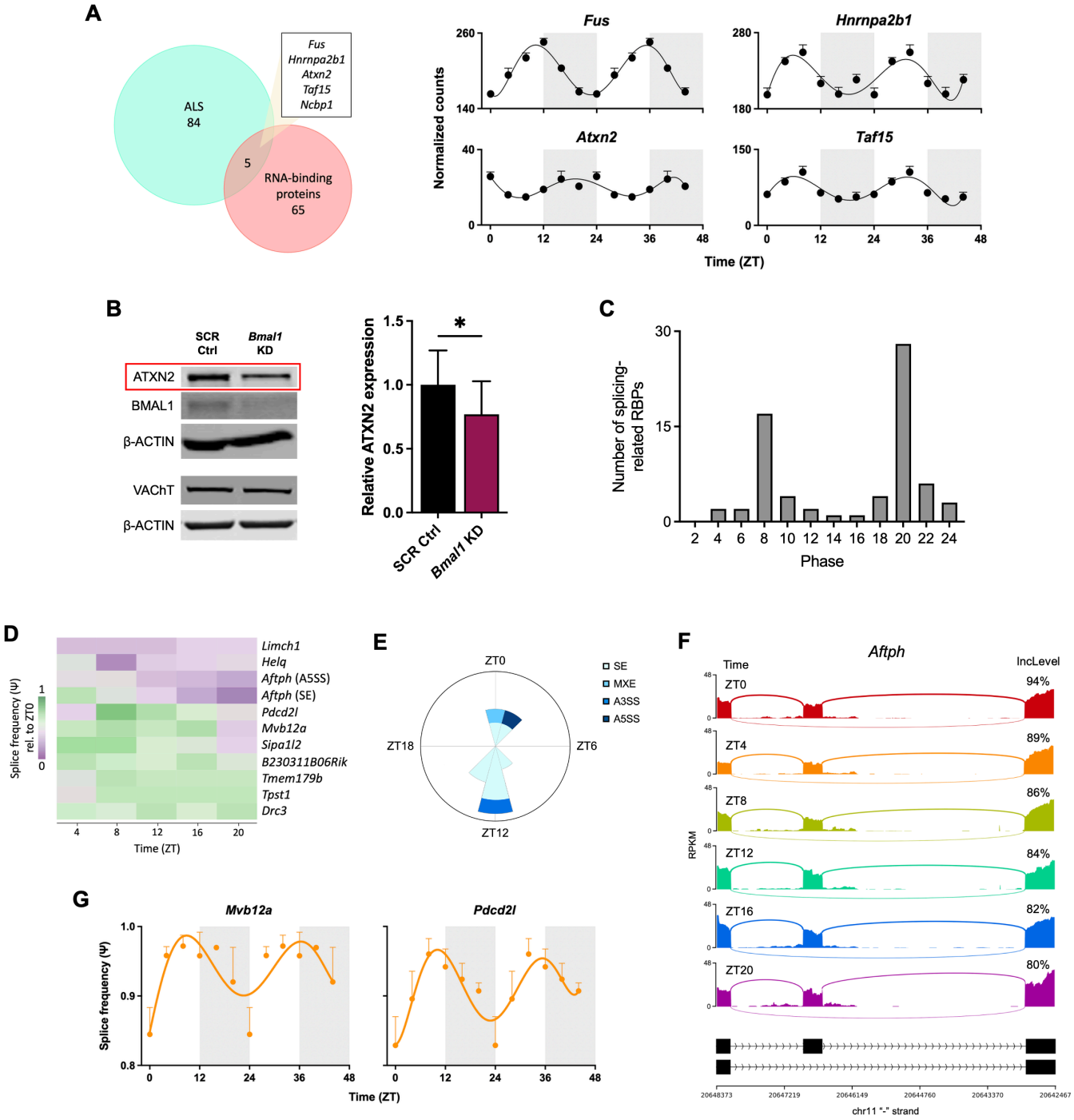

Figure 2. Circadian clock regulates expression of ALS-linked RBPs and alternative splicing in spinal cord cholinergic neurons. (A) Rhythmically expressed genes that encode ALS-linked RNA-binding proteins (RBPs) in WT spinal cord cholinergic neurons from 10-week-old *ChAT-Cre*;*RiboTag*$^{fx/+}$ male mice, shown as normalized counts identified through DESeq2 (n = 3 per time point). **(B)** Representative immunoblot showing ATXN2 protein expression in primary rat spinal cord cholinergic

neurons with siRNA knockdown of *Bmal1* vs. scramble (SCR) control ($n = 4$). VAChT was used to confirm the integrity of cholinergic neurons. Statistical significance was calculated by unpaired two-tailed Student's *t*-test (*$p < 0.05$). **(C)** Peak phase in expression of oscillating RBPs in WT cholinergic neurons within the GO term "RNA splicing." **(D)** Heatmap showing rhythmically spliced genes in WT cholinergic neurons obtained using rMATS splicing analysis, represented as splice frequency (Ψ) relative to ZT0 ($n = 3$ per time point). **(E)** Radial histogram showing the number of each type of rhythmic splicing event in WT cholinergic neurons with peak Ψ occurring within each 2-hr window. Radius corresponds to 4 splicing events. SE, skipped exon; MXE, mutually exclusive exon; A3SS and A5SS, alternative 3' and 5' splice sites. **(F)** Sashimi plots showing time-of-day-dependent alternative splicing of *Aftph* by SE every 4 h across the 24-hr day in WT cholinergic neurons, with exon inclusion levels indicated at each time point. **(G)** Rhythmic splice frequency graphs of the genes that are both rhythmically expressed and rhythmically spliced in WT cholinergic neurons. For A and G, data are represented as mean ± SEM and double-plotted for better visualization. Rhythmicity was determined by JTK_Cycle analysis (adjusted *p*-value < 0.05). The shaded regions denote the dark/active time periods.

Cholinergic neuron circadian clock regulates sALS-associated cytoskeleton, ECM, and NMJ gene expression

The circadian clock regulates a number of physiological processes, including sleep/wake activity, hormone secretion, and glucose homeostasis (Lowrey and Takahashi 2004; Rudic et al. 2004). Disrupting the clock through whole-body knockout or mutation of clock activators leads to metabolic dysfunction, accelerated aging, and neurodegenerative phenotypes (Englund et al. 2009; Garcia et al. 2000; Kondratov et al. 2006; Takahashi et al. 2008). Given the involvement of the cholinergic neuron clock in mediating neurodegenerative processes, we next sought to investigate the transcriptomic consequences of clock disruption through cholinergic neuron-specific deletion of clock activator BMAL1 at ZT8 (light period) and ZT20 (dark period), the times at which oscillating transcripts reached maximal abundance in opposing phases (Fig. 1C, 3A, and S1A-C).

We found 48 upregulated genes and 21 downregulated genes in *ChAT-BKO* neurons (*Bmal1*-knockout cholinergic neurons isolated from *ChAT-Cre;RiboTag*$^{fx/+}$*;Bmal1*$^{fx/fx}$ mice) compared to controls (WT cholinergic neurons isolated from *ChAT-Cre;RiboTag*$^{fx/+}$ mice) at ZT8, and 74 upregulated genes and 12 downregulated genes in *ChAT-BKO* neurons at ZT20 (Fig. 3B and 3D; Table S3A-B). KEGG, GO, and Reactome functional pathway analyses revealed over-representation for extracellular matrix (ECM) and cytoskeleton organization as well as immune response terms among the upregulated genes at both time points, along with enrichment for muscle-related processes among the upregulated genes at ZT20 (Fig. 3C and 3E-F). The cytoskeleton plays an important role in axonal transport and synaptic integrity, and cytoskeletal defects are prominent in ALS patients as well as disease models (Clark et al. 2016; Gall et al. 2020). Furthermore, ECM and cytoskeleton crosstalk is crucial for normal cell adhesion and migration processes, and both transcriptomic and proteomic studies have noted dysregulation of ECM biology in ALS samples (Geiger et al. 2001; Lin et al. 2020; Milioto et al. 2024; Qiu et al. 2014). The prevalence of cytoskeleton and ECM-associated genes within the differentially expressed genes in *Bmal1*-deficient cholinergic neurons suggests that clock disruption drives a restructuring that may contribute to similar deficits in axonal transport, synaptic integrity, and cell adhesion. Further, deletion of *Bmal1* at ZT20 induced the expression of genes within the GO term “muscle system process” (Fig. 3F),

which suggests that clock disruption during the dark/active period may influence neuromuscular junction (NMJ) dynamics. Enrichment for circadian rhythms appeared in the up- and down- regulated genes at both time points, as BMAL1 is a component of the core clock molecular feedback loop and its dysregulation influences the abundance of other clock genes (Table S3C).

Notably, our data revealed an increase in gene expression of the ionotropic glutamate receptor *N*-methyl-D-aspartate (NMDA) subunit *Grin2c* in *ChAT-BKO* cholinergic neurons at ZT20 (Fig. 3G). *Grin2c* was also found to be an RNA target of ALS-linked RBP FUS in mouse brain (Table S7) (Lagier-Tourenne et al. 2012). We previously showed that most rhythmic genes reach maximal abundance during the dark/active period and that there is enrichment of these genes for energy demanding processes (Fig. 1C and S2); our findings here suggest that clock disruption at ZT20 may alter cholinergic neuron bioenergetic balance in a manner that increases glutamate demand. Glutamate is the most abundant excitatory neurotransmitter in the CNS, and glutamate excitotoxicity—or the excess release of glutamate and overstimulation of glutamate receptors—is associated with motor neuron death in ALS and other neurodegenerative diseases (Bosch et al. 2006; Foran and Trotti 2009). We further observed time-of-day-dependent expression of genes encoding NMDA receptor subunits *Grin1*, *Grina*, and *Grin2b* (Fig. 3G), which may reflect how cholinergic neurons respond to fluctuations in glutamate release and demand throughout the day. These findings could have important implications for the timing and dosage of ALS drugs, such as riluzole, which utilizes sodium channel blockade to inhibit glutamatergic neurotransmission and excitotoxicity (Arnold et al. 2024; Nagoshi et al. 2015).

Figure 3

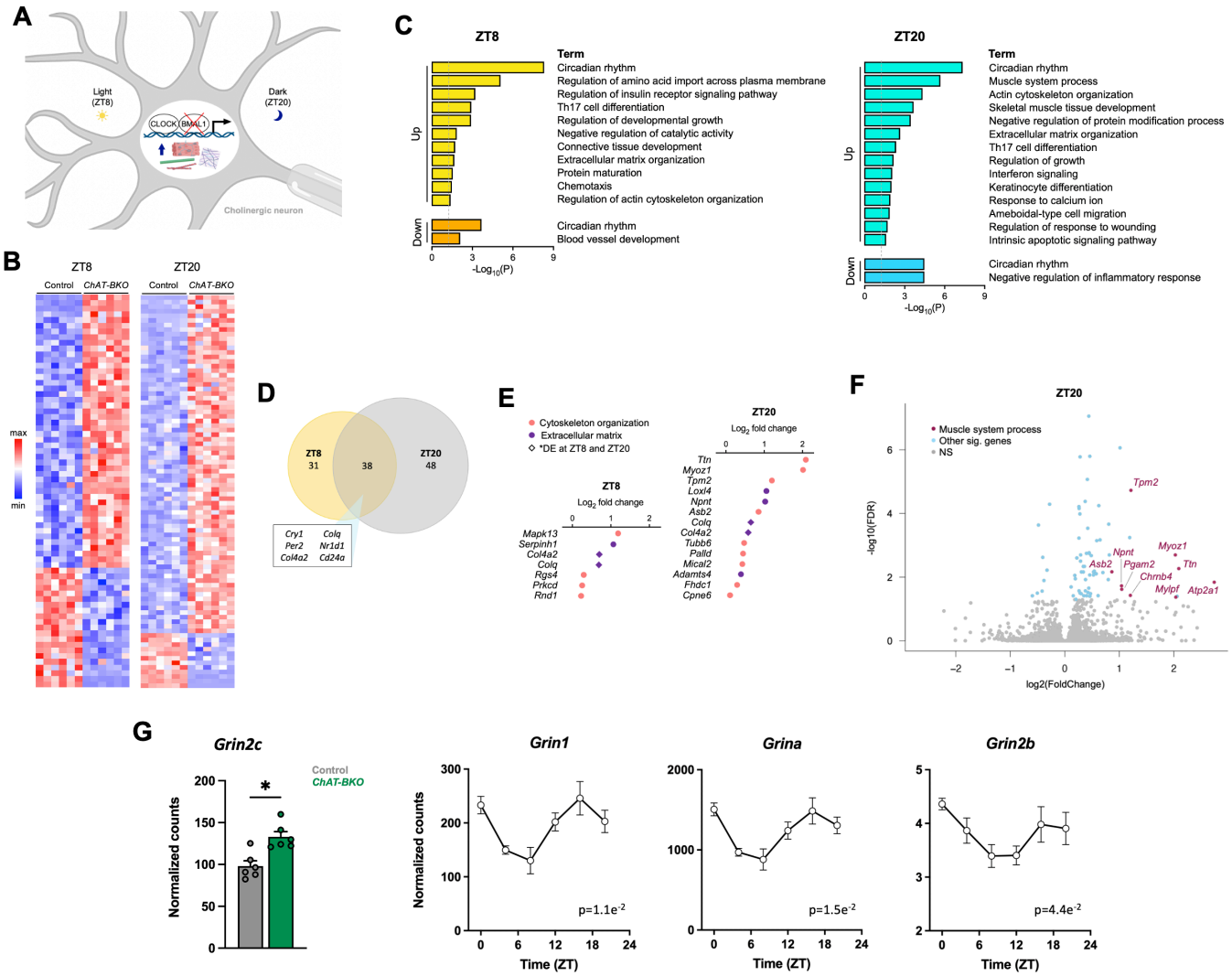

Figure 3. Cholinergic neuron circadian clock regulates cytoskeleton, ECM, and NMJ gene expression. (A) Model of cholinergic neuron-specific deletion of BMAL1 during the light (ZT8) and dark (ZT20) periods to induce the expression of cytoskeleton, extracellular matrix (ECM), and neuromuscular junction (NMJ) genes. Created using BioRender. **(B)** Heatmaps showing differentially expressed genes between *ChAT-BKO* (*Bmal1*-knockout cholinergic neurons isolated from *ChAT-Cre;RiboTag*$^{fx/+}$*;Bmal1*$^{fx/fx}$ mice) and control (WT cholinergic neurons isolated from *ChAT-Cre;RiboTag*$^{fx/+}$ mice) neurons from 6-month-old male mice at ZT8 and ZT20 (n = 6 per condition). **(C)** KEGG, GO, and Reactome functional pathway analyses of genes that are up- or down- regulated in *ChAT-BKO* cholinergic neurons vs. controls at ZT8 and ZT20. **(D)** Overlap of differentially expressed genes in *ChAT-BKO* cholinergic neurons at ZT8 and ZT20. **(E)** Increased expression of GO or literature-defined genes associated with cytoskeleton organization and ECM in *ChAT-BKO* cholinergic neurons at ZT8 and ZT20. **(F)** Volcano plot showing induction of NMJ genes within the GO term "muscle system process" in *ChAT-BKO* cholinergic neurons

at ZT20. **(G)** Induction of glutamate receptor NMDA subunit *Grin2c* in *ChAT-BKO* cholinergic neurons at ZT20 (n = 6 per condition) and time-of-day-dependent expression of genes encoding other NMDA subunits (n = 3 per time point), shown as normalized counts identified through DESeq2. Data are represented as mean ± SEM. Statistical significance was calculated using the Wald test with Benjamini-Hochberg correction for multiple comparisons (*adjusted $p < 0.05$) and rhythmicity was determined by JTK_Cycle analysis (adjusted p-value shown).

To next determine whether transcriptomic findings in mouse cholinergic neurons can be translated to humans, we performed *in silico* analysis of RNA-seq data from ALS patients and found that gene expression profiles altered in disease correspond with rhythmic gene networks. In analyzing lumbar spinal cord motor neurons from 13 sporadic ALS (sALS) patients and 8 healthy controls (Krach et al. 2018), we found 1,270 upregulated genes and 318 downregulated genes (Fig. 4A; Table S4A). KEGG, GO, and Reactome functional pathway analyses revealed over-representation of genes associated with ECM, cytoskeleton organization, and immune response among the upregulated genes (Fig. S4A), and enrichment of genes broadly linked to cytoskeleton dynamics and synaptic activation among the downregulated genes (Fig. S4B).

Gene set enrichment analysis (GSEA) showed that the orthologous upregulated genes in *ChAT-BKO* mouse cholinergic neurons at both ZT8 and ZT20 tended to be significantly upregulated in sALS patient LMNs as well (Fig. 4B). Through hypergeometric testing, we found overlap and enrichment of several upregulated genes in *ChAT-BKO* mouse cholinergic neurons among upregulated genes in sALS patient LMNs, including ECM organization genes *COL4A2* and *COLQ*, actin cytoskeleton gene *PALLD*, core clock repressor gene *CRY1*, and fatty acid elongation factor *ELOVL7* (Fig. 4C; Table S4B and S4C). Further, our analysis revealed upregulation of actin filament stabilization gene *TPM2* and cytoskeleton-regulating gene *PLA2G7* with *Bmal1*-loss at ZT20 (Lehtinen et al. 2017), as well as over-representation of these genes among the upregulated genes in sALS patient LMNs (Fig. 4D). We did not observe enrichment of downregulated genes in *ChAT-BKO* mouse cholinergic neurons among downregulated genes in sALS patient LMNs or enrichment of up- or down- regulated genes among sALS patient differentially expressed genes with opposite directionality (Table S4B). Our findings highlight the overlapping transcriptomic changes driven by clock disruption and neurodegenerative disease and reiterate the importance of ECM and cytoskeleton organization in neuronal health.

ALS-linked mutations disrupt RNA processing events, including mRNA axonal transport and local translation (Kapeli et al. 2017; Nagano and Araki 2021). Local translation enables the production of specific proteins when and where they are required, such as at synapses, where this process is critical for maintaining synaptic integrity and neurotransmission (Das et al. 2021; Jung et al. 2020). Notably, we

found significant enrichment of 59 orthologous downregulated genes in sALS patient LMNs associated with axonal transport (e.g., *Nefl*, *Tuba1a*, and *Mapk8ip3*) and NMJ synaptic regulation (e.g., *Grin2b*, *Atp8a2*, and *Herc1*) among rhythmic genes in WT mouse cholinergic neurons (Fig. 4E; Table S4D). While our analysis revealed 112 genes that were both upregulated in sALS patient LMNs and rhythmically expressed in WT mouse cholinergic neurons (Table S4E), there was no significant enrichment of orthologous sALS patient upregulated genes (1,183 genes) among the WT mouse rhythmic genes (adjusted p = 0.99 in hypergeometric test). Collectively, these findings suggest that there is circadian regulation of sALS-associated processes on the mRNA level and support a role for the cholinergic neuron clock in mediating ALS disease phenotypes.

Figure 4

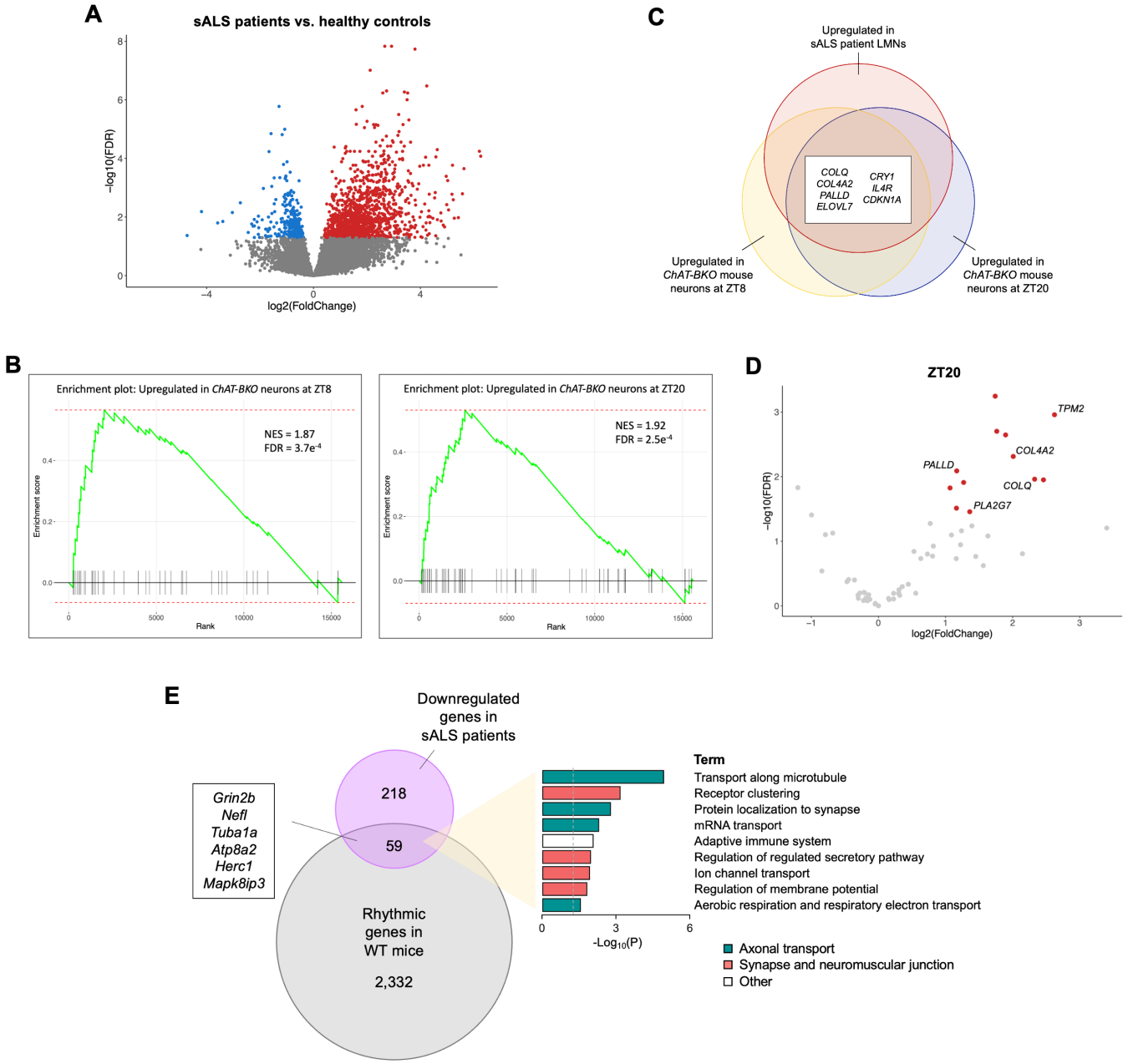

Figure 4. Cholinergic neuron circadian clock regulates sALS-associated cytoskeleton, ECM, and NMJ gene expression. (A) Volcano plot showing differentially expressed genes between sALS patient lumbar spinal cord motor neurons (*n* = 13) and healthy controls (*n* = 8). Re-analysis of data set from Krach et al. 2018. **(B)** GSEA plots showing enrichment of orthologous upregulated genes in *ChAT-BKO* neurons (*Bmal1*-knockout cholinergic neurons isolated from 6-month-old male *ChAT-Cre;RiboTag*$^{fx/+}$*;Bmal1*$^{fx/fx}$ mice) at ZT8 and ZT20 among rank-ordered genes in sALS patient LMNs (normalized enrichment score [NES] and false discovery rate [FDR]-adjusted *p*-value shown). **(C)**

Orthologous upregulated genes in *ChAT-BKO* mouse neurons at ZT8 and ZT20 that are over-represented among upregulated genes in sALS patient LMNs (adjusted $p < 0.01$ in hypergeometric tests at both time points). **(D)** Volcano plot of orthologous upregulated genes in *ChAT-BKO* mouse neurons at ZT20 that are significantly enriched among upregulated genes in sALS patient LMNs. **(E)** Enrichment of orthologous sALS patient LMN downregulated genes (277 genes) associated with axonal transport and NMJ synaptic regulation among rhythmic genes in WT mouse cholinergic neurons (adjusted $p < 0.01$ in hypergeometric test). LMN, lower motor neuron.

Cholinergic neuron-specific *Bmal1*-deletion drives neurodegeneration in lumbar spinal cord and sciatic nerve but does not alter mouse metabolic indices

Extensive loss of LMNs in the spinal cord and brain stem is a key neuropathological feature of ALS (Grad et al. 2017). Based on our transcriptomic analysis indicating a role for the cholinergic neuron clock in mediating neurodegenerative processes, we hypothesized that clock disruption may affect motor neuron health and survival. To test this, we performed Nissl staining and morphometric quantification of LMNs, with the criteria for motor neuron designation being neurons located in the ventral horn with cell bodies between 30-70μm in diameter, the presence of a multi-polar structure, and a visible nucleolus. We found a significant decrease in the number of motor neurons in lumbar spinal cord sections from mice with cholinergic neuron-specific *Bmal1*-deletion (*ChAT-Cre;Bmal1*$^{fx/fx}$ mice) compared to those from controls (*Bmal1*$^{fx/fx}$ mice) (20% decrease in median counts) (Fig. 5A-G).

Figure 5

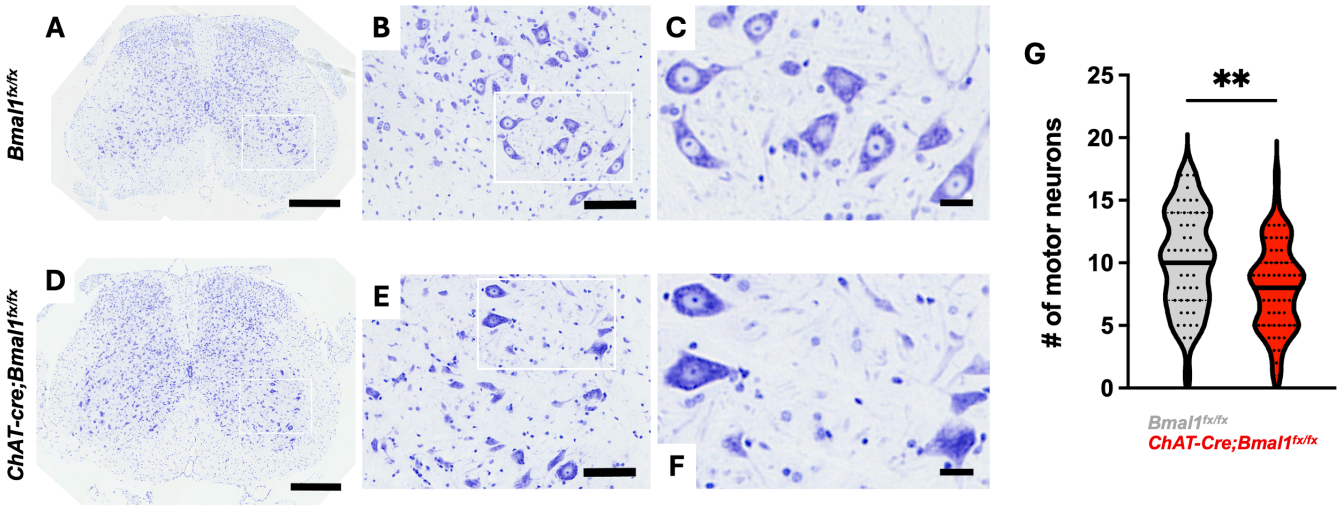

Figure 5. Cholinergic neuron-specific *Bmal1*-deletion drives lumbar spinal cord motor neuron loss. (A-F) Representative images of Nissl-stained lumbar spinal cord sections from 5–7-month-old male mice with cholinergic neuron-specific *Bmal1*-deletion (*ChAT-Cre*;*Bmal1*$^{fx/fx}$ mice) (D-F) and controls (*Bmal1*$^{fx/fx}$ mice) (A-C). Scale bars represent 400μm (A and D), 100μm (B and E), and 25μm (C and F). **(G)** Quantification of motor neurons per lumbar spinal cord section in *ChAT-Cre;Bmal1*$^{fx/fx}$ and *Bmal1*$^{fx/fx}$ mice (n = 5-6). Data are represented as median with interquartile range. Statistical significance was calculated by unpaired two-tailed Student's t-test (**$p < 0.01$).

The sciatic nerve enables cholinergic neuron innervation of hindlimb skeletal muscle at the NMJ, and sciatic nerve axon damage is associated with muscle denervation and ALS disease progression (Gordon et al. 2009; Moloney et al. 2014). Given the involvement of the clock in synaptic transmission (Gizowski et al. 2016; Marcheva et al. 2020), we next sought to test whether clock disruption alters NMJ innervation through changes to the sciatic nerve. We performed toluidine blue staining and transmission electron microscopy (TEM) to visualize alterations in sciatic nerve morphology. We observed a significant increase in the number of severely degenerated axons in mice with *Bmal1*-loss (122% increase in average counts), as characterized by expansion of the myelin sheath and axoplasmic abnormalities, such as shrinkage of the axoplasm (Fig. 6A-D) (Anderson et al. 2016; Essawy et al. 2011; Muzio et al. 2020). Axon degeneration is an intrinsic self-destruction mechanism that leads to axon loss during injury or disease, and the NAD^+ hydrolase SARM1 was found to promote axonal degeneration (Gerdts et al. 2015). Of note, our data revealed that *Sarm1* mRNA is rhythmically expressed and potentially clock-regulated in spinal cord cholinergic neurons (adjusted $p < 0.001$) (Table S1A). In line with our transcriptomic analysis of *Bmal1*-deficient cholinergic neurons, we demonstrate morphological changes to sciatic nerve axons that may contribute to altered NMJ dynamics.

Figure 6

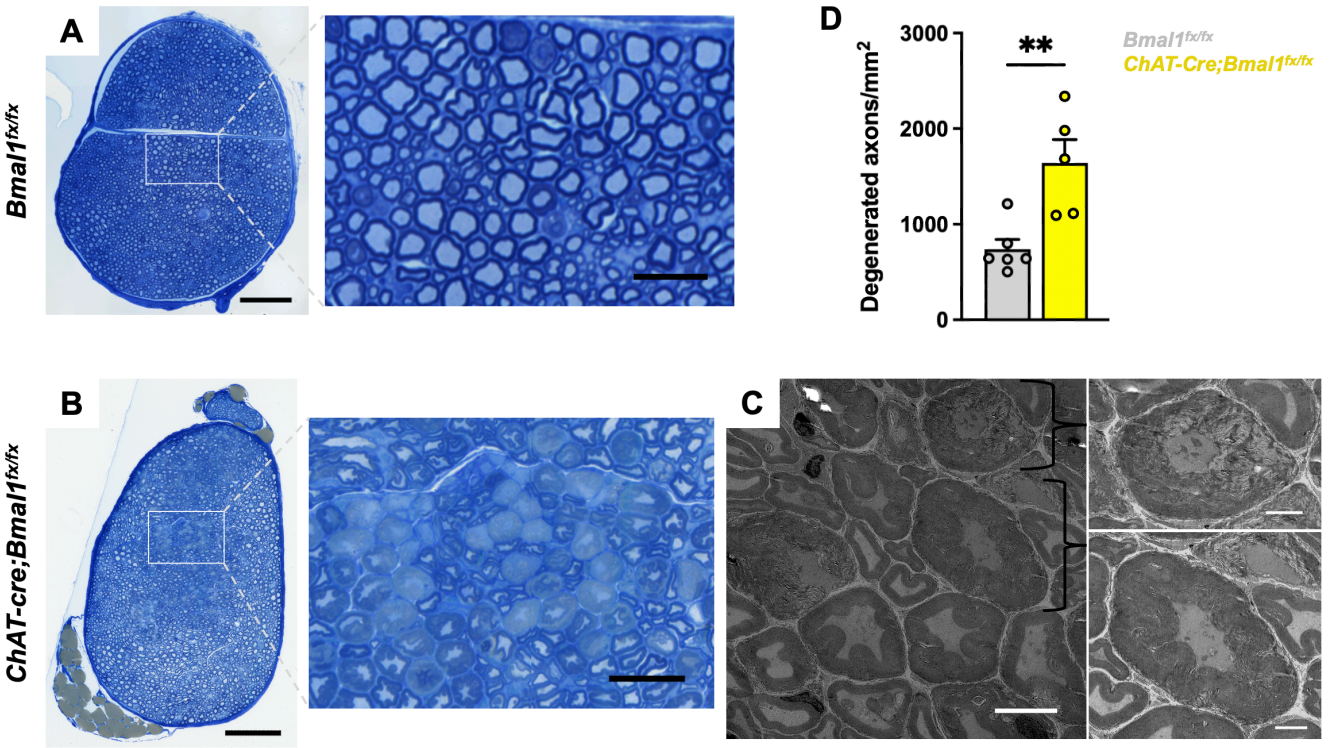

Figure 6. Cholinergic neuron-specific *Bmal1*-deletion increases axon degeneration in sciatic nerve. (A and B) Representative images of toluidine blue-stained sciatic nerve sections from 5–7-month-old male mice with cholinergic neuron-specific *Bmal1*-deletion (*ChAT-Cre*;*Bmal1*$^{fx/fx}$ mice) (B) and controls (*Bmal1*$^{fx/fx}$ mice) (A). Scale bars represent 100µm and 25µm (magnified view). **(C)** Transmission electron microscopy (TEM) images of degenerated axons from *ChAT-Cre*;*Bmal1*$^{fx/fx}$ mice shown in B. Scale bars represent 5µm and 2µm (magnified view). **(D)** Quantification of degenerated axons per sciatic nerve section (measured in mm^2) in *ChAT-Cre;Bmal1*$^{fx/fx}$ and *Bmal1*$^{fx/fx}$ mice (n = 5-6). Data are represented as mean ± SEM. Statistical significance was calculated by unpaired two-tailed Student's *t*-test (**$p < 0.01$).

Circadian behavior includes rhythmic patterns of locomotor activity, respiration, and feeding (Bass and Takahashi 2010), yet none of these parameters appeared to be altered with cholinergic neuron-specific *Bmal1*-deletion (Fig. S5A-C). Therefore, we postulate that the cellular pathologies observed with cholinergic neuron clock disruption arise due to cell-autonomous defects. Further, we did not observe changes in mouse whole-animal body or spinal cord weights (Fig. S5D-E).

Cholinergic neuron-specific *Bmal1*-deletion drives alternative splicing of ALS-linked RBPs and genes associated with RNA metabolism

Given that circadian timing plays a role in RBP expression and alternative splicing in cholinergic neurons, we next investigated whether clock disruption through *Bmal1*-deletion during the light and dark periods drives changes in splicing. Our analysis of *ChAT-BKO* cholinergic neurons harvested at ZT8 and ZT20 revealed 60 alternative splicing events across 49 unique genes during the light period, consisting of 34 SE, 5 MXE, 12 A3SS, and 9 A5SS (Fig. 7A and 7C; Table S5A-D), and 50 alternative splicing events across 41 unique genes during the dark period, consisting of 37 SE, 1 MXE, 4 A3SS, and 8 A5SS (Fig. 7A and 7C; Table S6A-D). We uncovered differentially spliced genes with multiple transcript variants in cholinergic neurons with *Bmal1*-loss, including ALS-associated genes *Stk16* (at ZT8) and *Atg10* (at ZT20), both of which underwent multiple exon skipping events (Fig. 7B) (García-García et al. 2021; Lee et al. 2015; Wang et al. 2019; Zhao et al. 2017). Microtubule-associated protein gene *Ccdc74a* and histone variant encoding gene *H2az2* were the only overlapping alternatively spliced genes between the two time points (Fig. 7C).

Functional pathway analysis revealed enrichment for the regulation of mRNA stability and RNA splicing as the top terms among the genes that were differentially spliced in *ChAT-BKO* neurons at ZT8 and ZT20, respectively (Fig. 7D), which suggests that *Bmal1*-deletion in cholinergic neurons alters RNA metabolism. In addition to alternative splicing, RNA processing includes mRNA axonal transport along microtubules as well as local translation at synapses to enable efficient neurotransmission (Kapeli et al. 2017; Nagano and Araki 2021). Deletion of *Bmal1* at ZT8 also resulted in altered splicing of several key genes related to mRNA stability, microtubule dynamics and transport, and postsynaptic organization (Fig.

7E). Notably, *Ythdf2* was alternatively spliced by SE with *Bmal1*-loss at ZT8 (Fig. 7E). *Ythdf2* encodes the N6-methyladenosine (m6A) reader protein YTHDF2, which is an RBP that recognizes and directs m6A-modified RNAs; its dysregulation has been implicated in a number of neurological disorders (Song et al. 2024). Further, YTHDF2 was found to accumulate in ALS spinal cord neurons and facilitate TDP-43-linked toxicity, and YTHDF2 knockdown prolonged the survival of human neurons with ALS-linked mutations (McMillan et al. 2023). In another example, we found that *Kif3a* was alternatively spliced by MXE with *Bmal1*-loss at ZT8 (Fig. 7E). *Kif3a* encodes the kinesin family molecular motor protein KIF3A, which was found to be reduced in sALS patient motor cortex (Hirokawa et al. 2009; Pantelidou et al. 2007). Interestingly, most of the alternatively spliced genes were distinct between the two time points assessed, and the alternatively spliced genes with *Bmal1*-deletion at ZT20 were enriched for a different set of pathways, including ubiquitin-dependent protein catabolic process and response to cellular stress (Fig. 7D). This demonstrates that there are time-of-day-dependent differences in cholinergic neuron circadian clock-mediated regulation of alternative splicing.

Figure 7

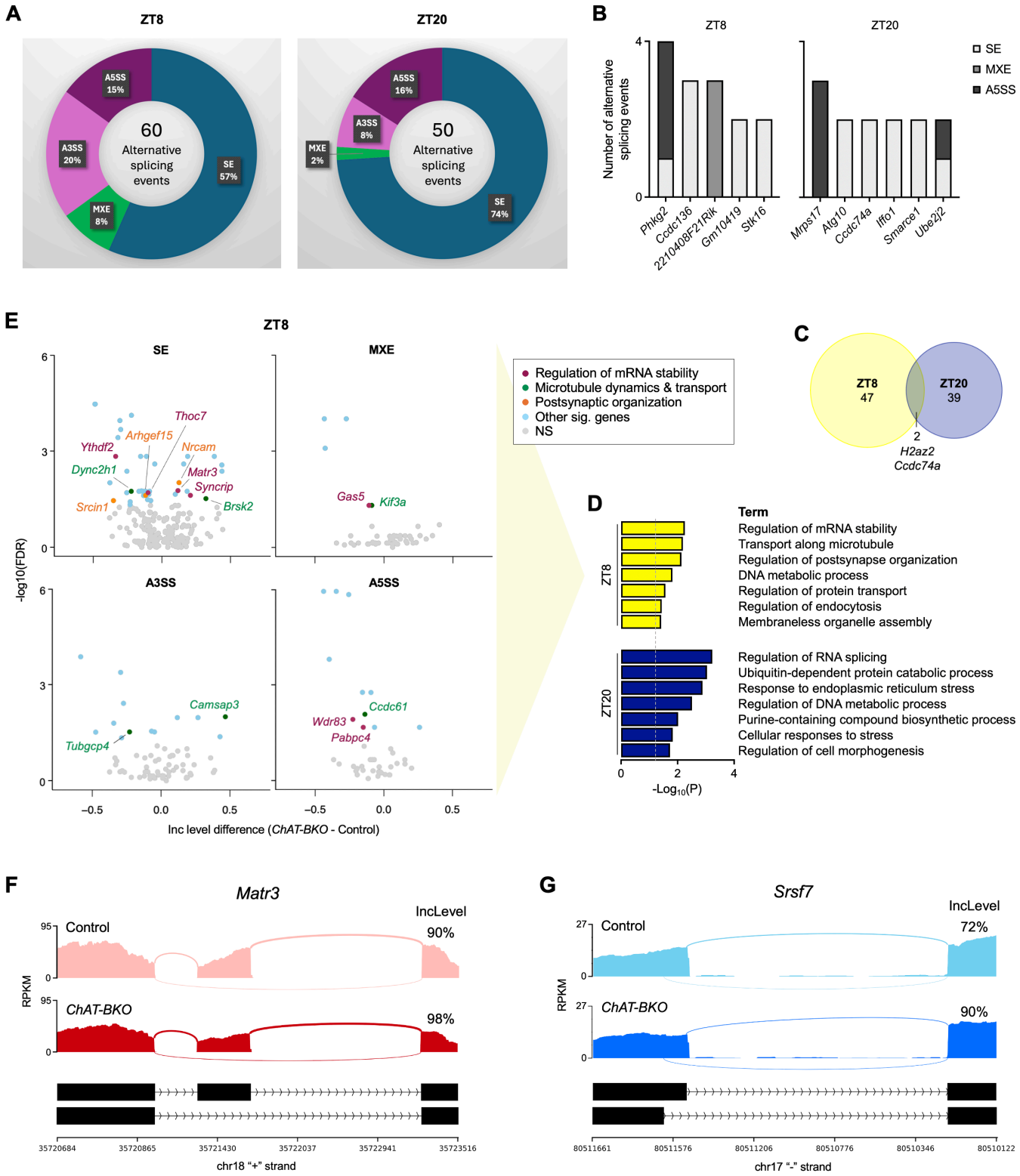
A
ZT8
A5SS 15%
A3SS 20%
MXE 8%
SE 57%
60 Alternative splicing events
ZT20
A5SS 16%
A3SS 8%
MXE 2%
SE 74%
50 Alternative splicing events
B
ZT8
ZT20
Number of alternative splicing events
SE
MXE
A5SS
Phkg2
Ccdc136
2210408F21Rik
Gm10419
Stk16
Mrps17
Atg10
Ccdc74a
Iffo1
Smarce1
Ube2j2
E
ZT8
SE
MXE
A3SS
A5SS
-log10(FDR)
Thoc7
Arhgef15
Ythdf2
Nrcam
Dync2h1
Matr3
Syncrip
Srcin1
Brsk2
Gas5
Kif3a
Camsap3
Tubgcp4
Ccdc61
Wdr83
Pabpc4
Inc level difference (ChAT-BKO - Control)
Regulation of mRNA stability
Microtubule dynamics & transport
Postsynaptic organization
Other sig. genes
NS
C
ZT8 47
ZT20 39
2
H2az2
Ccdc74a
D
Term
ZT8
Regulation of mRNA stability
Transport along microtubule
Regulation of postsynapse organization
DNA metabolic process
Regulation of protein transport
Regulation of endocytosis
Membraneless organelle assembly
ZT20
Regulation of RNA splicing
Ubiquitin-dependent protein catabolic process
Response to endoplasmic reticulum stress
Regulation of DNA metabolic process
Purine-containing compound biosynthetic process
Cellular responses to stress
Regulation of cell morphogenesis
-Log10(P)
F
Matr3
Control
IncLevel
90%
ChAT-BKO
98%
RPKM
35720684
35720865
35721430
35722037
35722941
35723516
chr18 "+" strand
G
Srsf7
Control
IncLevel
72%
ChAT-BKO
90%
RPKM
80511661
80511576
80511206
80510776
80510346
80510122
chr17 "-" strand

Figure 7. Cholinergic neuron-specific *Bmal1*-deletion drives alternative splicing of ALS-linked RBPs and genes associated with RNA metabolism. (A) Alternative splicing events in *ChAT-BKO* (*Bmal1*-knockout cholinergic neurons isolated from *ChAT-Cre;RiboTag*$^{fx/+}$*;Bmal1*$^{fx/fx}$ mice) and control (WT cholinergic neurons isolated from *ChAT-Cre;RiboTag*$^{fx/+}$ mice) neurons from 6-month-old male mice at ZT8 and ZT20 determined by rMATS analysis (n = 6 per condition). **(B)** Differentially spliced genes with multiple transcript variants in *ChAT-BKO* cholinergic neurons at ZT8 and ZT20. **(C)** Overlap of alternatively spliced genes in *ChAT-BKO* cholinergic neurons at ZT8 and ZT20. **(D)** KEGG, GO, and Reactome functional pathway analyses of alternatively spliced genes in *ChAT-BKO* cholinergic neurons at ZT8 and ZT20. **(E)** Volcano plots of alternatively spliced genes by SE, MXE, A3SS, and A5SS in *ChAT-BKO* cholinergic neurons at ZT8, including several associated with mRNA stability, microtubule dynamics and transport, and postsynaptic organization. **(F and G)** Sashimi plots showing altered splicing of ALS-linked RBPs *Matr3* by SE in *ChAT-BKO* cholinergic neurons at ZT8 (F) and *Srsf7* by A5SS in *ChAT-BKO* cholinergic neurons at ZT20 (G), with exon inclusion levels indicated. SE, skipped exon; MXE, mutually exclusive exon; A3SS and A5SS, alternative 3' and 5' splice sites.

An early study comparing sALS lumbar spinal cord motor neurons to healthy controls noted little overlap between the differentially expressed and differentially spliced genes, positing that these cohorts of genes were largely distinct from one another (Rabin et al. 2009). Consistent with this finding, we did not see any overlap between the differentially expressed and differentially spliced genes in *ChAT-BKO* cholinergic neurons at either time point. Moreover, another report found minimal overlap between differentially expressed and differentially spliced genes in clock-disrupted pancreatic β-cells (0.6% and 4% overlap, respectively) (Marcheva et al. 2020). These findings support that changes in splicing and mRNA abundance are regulated by distinct mechanisms that are downstream of the molecular clock.

Importantly, our data revealed altered splicing of genes that regulate mRNA stability and splicing in *ChAT-BKO* cholinergic neurons, including RBP-encoding genes *Matr3*, *Syncrip*, and *Thoc7* at ZT8 (Fig. 7E) and *Srsf7*, *Snrnp70*, and *U2af2* at ZT20. Matrin 3 (MATR3) is an ALS-linked DNA- and RNA- binding protein that plays key roles in chromatin organization, RNA processing, and mediating NMDA-induced neuronal cell death (Coelho et al. 2015; Giordano et al. 2005; Salton et al. 2011). It functions as a repressor of exon inclusion during alternative splicing, and mutations have been associated with increased cryptic exon inclusion as well as inhibition of mRNA nuclear export (Boehringer et al. 2017; Coelho et al. 2015; Johnson et al. 2014b; Khan et al. 2024; Uemura et al. 2017). We found that *Matr3* was alternatively spliced in cholinergic neurons with *Bmal1*-deletion during the light period with increased inclusion of a skipped exon (Fig. 7F; Table S5A) corresponding to exon 16 in the human genome (GRCh38.p14; ENST00000509990.5; chr5:139273752-139329404) (Dyer et al. 2025). Interestingly, a recent case study linked duplications in *Matr3* exons 15 and 16 to ALS (Caputo et al. 2022). Our analysis further revealed that ALS-linked RBP serine/arginine-rich splicing factor 7 (SRSF7) was alternatively spliced by A5SS in cholinergic neurons with *Bmal1*-deletion during the dark period (Fig. 7G; Table S6D), with changes corresponding to an increase in inclusion level of an exon 5 coding variant in the human genome (GRCh38.p14; ENST00000409276.5; chr2:38744893-38751358) (Dyer et al. 2025). Of note, SRSF7 depletion was found to decrease the abundance of Stathmin 2 (STMN2), an ALS-associated microtubule binding protein important for axon maintenance and regeneration following injury (Beccari et al. 2025; Klim et al. 2019; López-Erauskin et al. 2024; Wang et al. 2025).

We establish that there is circadian clock regulation of the splicing of RBPs themselves—including RBPs associated with ALS—and that, because the alternatively spliced RBPs at ZT8 and ZT20 are distinct, this process is time-of-day-dependent. Importantly, we demonstrate that ALS-linked RBPs are rhythmically expressed in WT cholinergic neurons and that, with *Bmal1*-deletion, ALS-linked RBPs are differentially spliced. Given that RBP mutations are a hallmark of ALS and other neurological disorders, it would be interesting to consider how clock-dependent gene expression and splice variants of these RBPs contribute to their own dysregulation as well as their control of alternative splicing in health and disease.

DISCUSSION

Alternative splicing plays a crucial role in the generation of transcriptomic and proteomic diversity, especially in neuronal cells, whose complex and specialized functions render them particularly vulnerable to disruption. The circadian clock adds another layer of complexity to this process by modulating post-transcriptional events based on the time-of-day-specific energetic demands of each cell. Given the length of motor neuron axons (up to ~1 meter) and the extensive distances RNA cargo have to travel, motor neurons are uniquely susceptible to disturbances in RNA processing, including disruption of axonal transport and local synaptic translation. Disrupted homeostasis of RBP mediators of RNA metabolism through mutation often result in neurological and neurodegenerative disorders, such as ALS. In healthy cells, RBP-bound mRNA is packaged into ribonucleoprotein (RNP) granules that are transported by motor proteins (e.g., dyneins and kinesins) along microtubules to axon terminals for local translation (Maday et al. 2014). Local translation of targeted mRNAs enables the production of specific proteins when and where they are needed, such as at neuronal synapses in order to maintain synaptic function (Das et al. 2021; Jung et al. 2020). Translation is also mediated by cellular stress, and RBP mutations have been shown to promote the formation of aberrant RNP stress granules—membraneless organelles that undergo phase transitions from transient liquid droplets to irreversible solid states (Kiebler and Bassell 2006; Lin et al. 2015). These phase transitions inhibit RBPs from carrying out their normal functions.

Dysregulation of ALS-linked RBPs has been shown to disrupt multiple aspects of RNA metabolism. For example, ALS-linked FUS mutations were found to alter FUS regulation of a motor neuron survival factor SMN and inhibit its transport to axons (Groen et al. 2013) as well as impair RNP granule function by inducing phase transitions (Murakami et al. 2015; Patel et al. 2015). Further, ALS-linked mutations in TAF15 were found to increase the number of TAF15-positive axonal and dendritic stress granules (Couthouis et al. 2011), and inhibition of TAF15 methylation resulted in the accumulation of TAF15 in TIA1-positive stress granules (Jobert et al. 2009). Our investigation into the link between two central evolutionarily conserved processes, the circadian clock transcriptional program and alternative splicing, yields important insight into time-of-day-dependent mechanisms of RBP regulation and RNA metabolism in cholinergic neurons. We demonstrate clock-dependent expression of the RBP ATXN2, a known regulator of the circadian clock (Lim and Allada 2013; Zhang et al. 2013). In connection to neurodegenerative disease, polyglutamine (polyQ) repeat expansions in *ATXN2* cause spinocerebellar ataxia type 2 (SCA2) and increase the risk for development of ALS (Elden et al. 2010; Glass et al. 2022; Nussbacher et al. 2019). Pathogenic variants have been shown to aberrantly sequester TDP-43, inhibit mRNA transport and local translation, and reduce motor function and NMJ area (Vieira de Sá et al. 2024; Wijegunawardana et al. 2025). Of note, reduction of ATXN2 in transgenic mice was found to decrease TDP-43 aggregation and improve motor function and survival (Becker et al. 2017).

While our data support that neurodegenerative processes are mediated by the circadian clock in spinal cord cholinergic neurons—the cell-type of ALS disease pathogenesis—further investigation into how *Bmal1*-loss influences the localization and function of ALS-linked RBPs (e.g., TDP-43 and FUS), for example, would help establish a link between clock disruption and ALS-specific pathophysiology. In addition, functional analyses would be needed to inform causal relationships. Our work and previous studies demonstrating circadian regulation of alternative splicing in neurons as well as clock-dependent neurotransmission support that there may be clock-mediated RBP regulation of neurotransmitter release at motor neuron NMJ synapses (Gizowski et al. 2016; Marcheva et al. 2020; Shinohara et al. 2002; Wang et al. 2018). Cholinergic neurons release the neurotransmitter acetylcholine as a chemical messenger to transmit signals to other neurons and muscle cells in order to coordinate processes such as muscle

contraction; acetylcholinesterase (AChE) is an enzyme that plays key roles in NMJ formation and acetylcholine breakdown during signal termination (Campanari et al. 2016; Fernandez et al. 1986). Of note, decreased acetylcholine release due to motor neuron degeneration as well as decreased AChE activity in muscle and cerebrospinal fluid has previously been reported in ALS patients (Campanari et al. 2016; Drannik et al. 2017; Fernandez et al. 1986). Given the neurodegenerative phenotypes we observed along with our transcriptomic data demonstrating altered NMJ dynamics with *Bmal1*-deletion, it would be interesting to explore functional changes in acetylcholine and AChE levels in clock-disrupted spinal cord cholinergic neurons, especially in relation to changes in the rhythmically expressed ALS-linked RBPs (i.e., *Fus*, *Hnrnpa2b1*, *Atxn2*, *Taf15*, and *Ncbp1*).

We show that 70 splicing-related RBP transcripts are rhythmically expressed in spinal cord cholinergic neurons, including several that are directly linked to ALS (see above). Future studies should address whether any of these rhythmic RBPs regulate the alternatively spliced transcripts observed with *Bmal1*-deletion in this neuronal subtype. Previous cross-linking and immunoprecipitation followed by sequencing (CLIP-seq) studies and variations have identified RNA targets of disease-linked RBPs in neuronal tissue and cells, many of which we found to be rhythmically expressed or spliced in WT cholinergic neurons or differentially regulated in cholinergic neurons with *Bmal1*-deletion (Table S7). For instance, we note that actin stress fiber gene *Limch1* is both rhythmically spliced in cholinergic neurons and an overlapping target of rhythmically expressed ALS-linked RBPs FUS, TAF15, and hnRNPA2B1 (Table S7) (Ibrahim et al. 2013; Martinez et al. 2016; Nakaya et al. 2013), suggesting that one or more of these RBPs may directly regulate its RNA processing and protein function in a time-of-day-dependent manner. In another example, *Snrnp70* encodes an essential small nuclear ribonucleoprotein (snRNP) component of the spliceosome and is a target of both TAF15 and hnRNPA2B1 (Ibrahim et al. 2013; Martinez et al. 2016; Nikolaou et al. 2022; Wahl et al. 2009). Our results demonstrate that *Snrnp70* is rhythmically expressed in WT cholinergic neurons and differentially spliced in cholinergic neurons with *Bmal1*-deletion (Table S7), raising the possibility that circadian clock disruption alters TAF15 or hnRNPA2B1 regulation of *Snrnp70* in cholinergic neurons. Further insight into cell-type-specific RBP-

RNA interactions would inform how clock-dependent mechanisms contribute to alterations in RNA metabolism observed with neurological disease and provide insight into novel therapeutic avenues.

MATERIALS & METHODS

Animals

All animal procedures were conducted in accordance with regulations of the Institutional Animal Care and Use Committee at Northwestern University. All experiments were conducted using C57BL/6J mice maintained on a 12:12 light/dark cycle. WT cholinergic neuron isolation was achieved by crossing *ChAT-Cre* mice (gift from L. Parisiadou, Northwestern University; JAX #006410) (Rossi et al. 2011) with *RiboTag*$^{fx/fx}$ mice (obtained from Jackson Laboratories #029977) (Sanz et al. 2009) to generate *ChAT-Cre;RiboTag*$^{fx/+}$ mice. These experiments were performed using 10-week-old male mice. Cholinergic neuron-specific deletion of *Bmal1* was achieved by crossing *Bmal1*$^{fx/fx}$ mice (gift from J. Bass, Northwestern University) (Johnson et al. 2014a) with *ChAT-Cre* or *RiboTag*$^{fx/fx}$ mice to ultimately generate *ChAT-Cre;Bmal1*$^{fx/fx}$ mice (along with *Bmal1*$^{fx/fx}$ littermate controls) and *ChAT-Cre;RiboTag*$^{fx/+}$*;Bmal1*$^{fx/fx}$ mice (along with *ChAT-Cre;RiboTag*$^{fx/+}$ controls). These experiments were performed using 5–7-month-old male mice to assess the added insult of older age on phenotype and transcriptional program.

Protein gel electrophoresis and immunoblotting

Whole-cell lysates were prepared in RIPA lysis and extraction buffer (Thermo Scientific, 89900) supplemented with 1X Protease Inhibitor Cocktail (Sigma, P8340). Protein levels were quantified using Pierce BCA protein assay kit (Thermo Scientific, A65453). Protein extracts were then subjected to SDS-PAGE gel electrophoresis and transferred to nitrocellulose membranes (Bio-rad, 1620115). Primary antibodies used were BMAL1 (1:1,000 dilution; Cell Signaling, D2L7G), ATXN2 (1:2,000 dilution; Proteintech, 21776-1-AP), VAChT (1:1,000 dilution; Invitrogen, MA5-27662), and β-ACTIN (1:5,000 dilution; Novus Biologicals, NB600501). Species-specific IRDye secondary antibodies were used (1:10,000 dilution; LI-COR Biotech LLC).

Primary spinal cord motor neuron culture and siRNA transfection

Embryonic day 15 (E15) rat spinal cord was isolated and dissociated by incubation with 0.25% Trypsin-EDTA (Gibco, 25200056) for 15 min at 37°C. Samples were then centrifuged at 300 RCF for 10 min in Neurobasal media (Gibco, 21103049) containing B-27 (Gibco, A3582801), 2.5% DNase I, and 4% bovine serum albumin (BSA). Cells were resuspended by gentle up and down pipetting. The spin-resuspension process was then repeated. Motor neurons were enriched by adding 1mL BSA to the bottom of the resuspension tube. Cultures were then plated onto poly-lysine-coated plates and maintained in conditioned Neurobasal media containing 10% horse serum. On day *in vitro* (DIV) 1, primary neurons were transfected with either three siRNAs targeting the knockdown of *Bmal1* in equal proportion (Thermo Scientific, s131939-41) or Silencer Select Negative Control siRNA (Invitrogen, 4390843), using Lipofectamine RNAiMAX transfection reagent (Invitrogen, 13778150) and reduced serum Opti-MEM I (Gibco, 31985062) in antibiotic-free media. On DIV4, cultures were treated with 5μM AraC (Sigma, C6645) for 48 h to arrest astrocyte proliferation (Mojsilovic-Petrovic et al. 2009). On DIV14, neurons were collected for immunoblotting (as described above).

Lumbar spinal cord Nissl staining and morphometric quantification

Mice were anesthetized with intraperitoneal injection of Euthasol (390mg/mL pentobarbital sodium, 50mg/mL phenytoin sodium), and then transcardially perfused with phosphate-buffered saline (PBS) followed by 4% paraformaldehyde (PFA) in 0.4M phosphate buffer (pH 7.4). Lumbar spinal cord was isolated, post-fixed in the same fixative overnight at 4°C, and paraffin embedded. 6μm thick sections were cut and mounted onto slides. Samples were then deparaffinized and hydrated, prior to staining with heated Cresyl Violet acetate (Sigma, C5042) solution for 10 min and differentiation in 90% ethanol for 20 min. Finally, samples were dehydrated in ethanol, cleared in xylene, and mounted with DPX Mountant (Sigma, 06522). Tile stitched images at 20X magnification were acquired using TissueFAXS PLUS (TissueGnostics) to obtain whole spinal cord cross sections. After images were blinded, motor neurons were counted in every sixth section in an average of 11 sections per animal. Criteria for motor neuron

designation were neurons located in the ventral horn with cell bodies between 30-70μm in diameter, the presence of a multi-polar structure, and a visible nucleolus.

Sciatic nerve transmission electron microscopy and morphometric quantification

Mice were anesthetized with intraperitoneal injection of Euthasol (390mg/mL pentobarbital sodium, 50mg/mL phenytoin sodium), and then transcardially perfused with PBS followed by 4% PFA in 0.4M phosphate buffer (pH 7.4). Sciatic nerve was isolated and immersion-fixed in 0.1M sodium cacodylate buffer (pH 7.35) containing 2.5% glutaraldehyde and 2% PFA overnight at 4°C. Tissue was post-fixed in 2% osmium tetroxide, en bloc stained with 3% uranyl acetate, and dehydrated in ascending grades of ethanol followed by propylene oxide. Samples were then embedded in EMbed 812 Resin (Electron Microscopy Sciences, 14900) and cured overnight in a 60°C oven. 1μm thick sections were cut using the EM UC6 Ultramicrotome (Leica Microsystems) and stained with Toluidine Blue O. Tile stitched images at 40X magnification were acquired using TissueFAXS PLUS (TissueGnostics) to obtain whole nerve cross sections. After images were blinded, severely degenerated axons, characterized by expansion of the myelin sheath and axoplasmic abnormalities (e.g., shrinkage of the axoplasm) (Anderson et al. 2016; Essawy et al. 2011; Muzio et al. 2020) were counted within each nerve section and divided by the total area of the section (in mm^2). For transmission electron microscopy (TEM), ultrathin 70nm sections were mounted onto mesh copper grids and stained with uranyl acetate and Reynolds Lead Citrate. Images at 1,400X and 2,900X magnification levels were captured at 80 kV using Tecnai G2 Spirit (FEI Company) and Tecnai Imaging & Analysis Software.

Cholinergic neuron ribosome immunoprecipitation and RNA isolation

Spinal cord tissue was isolated and snap-frozen from 10-week-old *ChAT-Cre*;*RiboTag*$^{fx/+}$ mice at ZT0, 4, 8, 12, 16, and 20 or from 6-month-old *ChAT-BKO* (*ChAT-Cre;RiboTag*$^{fx/+}$*;Bmal1*$^{fx/fx}$) mice and controls (*ChAT-Cre;RiboTag*$^{fx/+}$) at ZT8 and ZT20. All samples for each experiment were processed on the same day. Homogenization buffer consisting of 1% sodium deoxycholate, 50mM Tris (pH 7.5), 100mM KCl, 12mM $MgCl_2$, 1% Tergitol (NP-40), 1mM dithiothreitol (DTT), 200U/mL RNasin Ribonuclease Inhibitor

(Promega, N2115), 1mg/mL heparin, 100µg/mL cycloheximide, and Protease Inhibitor Cocktail (Sigma, P8340) was made fresh and pre-chilled. One spinal cord was placed in a 2mL Dounce homogenizer vessel on ice with 2mL homogenization buffer, and homogenized with 30 strokes of 'pestle A' followed by 30 strokes of 'pestle B.' The homogenate was then centrifuged at 10,000 RCF for 10 min at 4°C. TRIzol Reagent (Invitrogen, 15596026) was added to 80µL of the spun homogenate and frozen at -80°C as pooled Input (RNA from whole spinal cord). 800µL of the remaining non-pelleted homogenate was incubated with 4µL of anti-HA antibody (BioLegend, 901514) for 4 hours at 4°C with end-over-end rotation. Samples were then incubated with 200µL of pre-washed protein A/G magnetic beads (Thermo Scientific Pierce, 88803) overnight at 4°C with end-over-end rotation. High salt buffer consisting of 50mM Tris (pH 7.5), 300mM KCl, 12mM $MgCl_2$, 1% NP-40, 0.5mM DTT, and 100µg/mL cycloheximide was made fresh and pre-chilled. Samples were placed on a magnetic stand on ice and washed three times with high salt buffer (800µL per wash) to remove non-specific binding from the immunoprecipitate (IP) product. After careful removal of high salt buffer, samples were treated with 700µL of TRIzol Reagent and frozen at -80°C until RNA was extracted using the Direct-zol RNA MicroPrep kit (Zymo Research Corp., R2062) following the manufacturer's instructions.

Library preparation and RNA sequencing

Following RNA isolation, RNA quality was assessed by Bioanalyzer (Agilent) and those with an RNA Integrity Number (RIN) greater than 7 were used for library prep. Libraries were constructed from 100 or 300 ng of RNA (for rhythmic or differential analyses, respectively) using the Illumina Stranded mRNA Prep kit (Illumina, 20040534) according to the manufacturer's instructions. Libraries were quantified by both Bioanalyzer (Agilent) and qPCR-based quantification (Kapa Biosystems). 150bp paired-end sequencing was performed on a NovaSeq X Plus (Illumina) to a minimum depth of 30M reads. Sequences were aligned to the mm10 transcriptome with STAR (v2.7.5) using the –quantMode Transcriptome and GeneCounts options. Gene counts were obtained from mm10 annotations (Ensembl 98) using rsem-calculate-expression (v1.3.0).

Differential expression, differential splicing, and rhythmicity analyses

Differential mRNA expression analysis was performed using DESeq2 (v1.32.0) after removal of genes with < 10 assigned counts. Differentially expressed transcripts were defined as having a false discovery rate (FDR)-adjusted *p*-value < 0.05. Alternative splicing analysis was performed using replicate multivariate analysis of transcript splicing (rMATS) (v4.0.2) (Shen et al. 2014) to quantify reads across annotated splice junctions present in the mm10 assembly. Differentially spliced transcripts were defined as having an FDR-adjusted *p*-value < 0.05 and a minimum exon inclusion level difference > 10%. Rhythmic mRNA expression and rhythmic splice frequency throughout the day were assessed by JTK_Cycle analysis (Hughes et al. 2010), allowing for period lengths of 20, 24, or 28 hours to account for 4-h sampling frequency. Rhythmicity was determined by an FDR-adjusted *p*-value < 0.05. KEGG, GO, and Reactome pathway enrichment analyses were performed using limma and biomaRt (v2.48.2), ShinyGO (v0.77) (Ge et al. 2019), Metascape (Zhou et al. 2019), and Cytoscape (Shannon et al. 2003). Certain plots were made in R (v4.0.3) using ggplot2 (v3.3.0), gplots (v3.1.1), pheatmap (v1.0.12), and fgsea (v1.16.0).

Statistical analysis

Results are presented as mean ± standard error of the mean (SEM) unless otherwise indicated. Statistical analyses were performed by unpaired two-tailed Student's *t*-test or analysis of variance (ANOVA) with corrections for multiple comparisons, where applicable. Hypergeometric tests were used to determine enrichment of genes from one dataset within another. The Wald test with Benjamini-Hochberg correction for multiple comparisons was used for statistical analysis of normalized count data from DESeq2. *P*-values < 0.05 were considered statistically significant. Detailed information on genotype, sample size, and *p*-value can be found within individual figures and figure legends.

Data access

All raw and processed sequencing data generated in this study have been deposited in the NCBI Gene Expression Omnibus under accession number GSE297457.

ACKNOWLEDGEMENTS

We thank C. Peek, M. Perelis, H-X. Deng, and members of the Kalb and Bass laboratories for helpful discussion. We also thank B. Weidemann for bioinformatics training, Y. Shi and H-X. Deng for spinal cord experimental techniques, and L. Reynolds Jr. for TEM assistance. We thank the Northwestern University Center for Genetic Medicine NUSeq Core, Northwestern University Comprehensive Metabolic Core, and Northwestern University Center for Advanced Microscopy (RRID: SCR_020996), supported by NCI CCSG P30 CA060553 awarded to the Robert H. Lurie Comprehensive Cancer Center. **Funding:** This research was supported by the US Public Health Service NS122908 and NS124802, the US Department of Defense W81XWH-21-1-0236, and the Heather Koster Family Charitable Fund (R.G.K.), NIH T32HL007909 and the Northwestern University Center for Sleep and Circadian Biology (S.B.T.), and the Les Turner ALS Foundation (R.G.K., E.K., S.B.T., J.M-P., E.M.B., and M.W.). E.K. is a New York Stem Cell Foundation Robertson Investigator. **Author contributions:** S.B.T. performed and analyzed all experiments with assistance from N.J.W., M.W., J.M-P., and E.M.B.; R.G.K., J.B., and E.K. supervised the study; S.B.T., J.B., and R.G.K. wrote and edited the manuscript. **Competing interests:** The authors declare no competing financial interests.

REFERENCES

Alami NH, Smith RB, Carrasco MA, Williams LA, Winborn CS, Han SSW, Kiskinis E, Winborn B, Freibaum BD, Kanagaraj A, et al. 2014. Axonal transport of TDP-43 mRNA granules is impaired by ALS-causing mutations. Neuron. 81:536-543. doi: 10.1016/j.neuron.2013.12.018. PMID: 24507191; PMCID: PMC3939050.

Anderson DM, Cannavino J, Li H, Anderson KM, Nelson BR, McAnally J, Bezprozvannaya S, Liu Y, Lin W, Liu N, et al. 2016. Severe muscle wasting and denervation in mice lacking the RNA-binding protein ZFP106. Proc Natl Acad Sci U S A. 113:E4494-4503. doi: 10.1073/pnas.1608423113. PMID: 27418600; PMCID: PMC4978283.

Andres-Alonso M, Ammar MR, Butnaru I, Gomes GM, Acuña Sanhueza G, Raman R, Yuanxiang P, Borgmeyer M, Lopez-Rojas J, Raza SA, et al. 2019. SIPA1L2 controls trafficking and local signaling of TrkB-containing amphisomes at presynaptic terminals. Nat Commun. 10:5448. doi: 10.1038/s41467-019-13224-z. PMID: 31784514; PMCID: PMC6884526.

Arnold FJ, Putka AF, Raychaudhuri U, Hsu S, Bedlack RS, Bennett CL, La Spada AR. 2024. Revisiting Glutamate Excitotoxicity in Amyotrophic Lateral Sclerosis and Age-Related Neurodegeneration. Int J Mol Sci. 25:5587. doi: 10.3390/ijms25115587. PMID: 38891774; PMCID: PMC11171854.

Bass J, Takahashi JS. 2010. Circadian integration of metabolism and energetics. Science. 330:1349-1354. doi: 10.1126/science.1195027. PMID: 21127246; PMCID: PMC3756146.

Bass J. 2012. Circadian topology of metabolism. Nature. 491:348-356. doi: 10.1038/nature11704. PMID: 23151577.

Beccari MS, Arnold-Garcia O, Baughn MW, Artates JW, McAlonis-Downes M, Lim J, Leyva-Cázares DF, Rubio-Lara HI, Ramirez-Rodriguez A, Bernal-Buenrostro CN, et al. 2025. Stathmin-2 enhances motor axon regeneration after injury independent of its binding to tubulin. Proc Natl Acad Sci U S A. 122:e2502294122. doi: 10.1073/pnas.2502294122. PMID: 40392845; PMCID: PMC12130871.

Becker LA, Huang B, Bieri G, Ma R, Knowles DA, Jafar-Nejad P, Messing J, Kim HJ, Soriano A, Auburger G, 2017. Therapeutic reduction of ataxin-2 extends lifespan and reduces pathology in TDP-43 mice. Nature. 544:367-371. doi: 10.1038/nature22038. PMID: 28405022; PMCID: PMC5642042.

Boehringer A, Garcia-Mansfield K, Singh G, Bakkar N, Pirrotte P, Bowser R. 2017. ALS Associated Mutations in Matrin 3 Alter Protein-Protein Interactions and Impede mRNA Nuclear Export. Sci Rep. 7:14529. doi: 10.1038/s41598-017-14924-6. PMID: 29109432; PMCID: PMC5674072.

Burman JL, Wasiak S, Ritter B, de Heuvel E, McPherson PS. 2005. Aftiphilin is a component of the clathrin machinery in neurons. FEBS Lett. 579:2177-2184. doi: 10.1016/j.febslet.2005.03.008. PMID: 15811338.

Campanari ML, García-Ayllón MS, Ciura S, Sáez-Valero J, Kabashi E. 2016. Neuromuscular Junction Impairment in Amyotrophic Lateral Sclerosis: Reassessing the Role of Acetylcholinesterase. Front Mol Neurosci. 9:160. doi: 10.3389/fnmol.2016.00160. PMID: 28082868; PMCID: PMC5187284.

Caputo M, Zucchi E, Martinelli I, Gianferrari G, Simonini C, Amedei A, Niccolai E, Gellera C, Pensato V, Mandrioli J. 2022. Duplication of exons 15 and 16 in Matrin-3: a phenotype bridging amyotrophic lateral sclerosis and immune-mediated disorders. Neurol Sci. 43:1419-1421. doi: 10.1007/s10072-021-05669-2. PMID: 34665352.

Chen M, Manley JL. 2009. Mechanisms of alternative splicing regulation: insights from molecular and genomics approaches. Nat Rev Mol Cell Biol. 10:741-754. doi: 10.1038/nrm2777. PMID: 19773805; PMCID: PMC2958924.

Clark JA, Yeaman EJ, Blizzard CA, Chuckowree JA, Dickson TC. 2016. A Case for Microtubule Vulnerability in Amyotrophic Lateral Sclerosis: Altered Dynamics During Disease. Front Cell Neurosci. 10:204. doi: 10.3389/fncel.2016.00204. PMID: 27679561; PMCID: PMC5020100.

Coelho MB, Attig J, Bellora N, König J, Hallegger M, Kayikci M, Eyras E, Ule J, Smith CW. 2015. Nuclear matrix protein Matrin3 regulates alternative splicing and forms overlapping regulatory networks with PTB. EMBO J. 34:653-668. doi: 10.15252/embj.201489852. PMID: 25599992; PMCID: PMC4365034.

Couthouis J, Hart MP, Shorter J, DeJesus-Hernandez M, Erion R, Oristano R, Liu AX, Ramos D, Jethava N, Hosangadi D, et al. 2011. A yeast functional screen predicts new candidate ALS disease genes. Proc Natl Acad Sci U S A. 108:20881-20890. doi: 10.1073/pnas.1109434108. Erratum in: Proc Natl Acad Sci U S A. 2023. 120:e2220845120. doi: 10.1073/pnas.2220845120. PMID: 22065782; PMCID: PMC3248518.

Das S, Vera M, Gandin V, Singer RH, Tutucci E. 2021. Intracellular mRNA transport and localized translation. Nat Rev Mol Cell Biol. 22:483-504. doi: 10.1038/s41580-021-00356-8. Erratum in: Nat Rev Mol Cell Biol. 2021. 22:505. doi: 10.1038/s41580-021-00374-6. PMID: 33837370; PMCID: PMC9346928.

Deng HX, Bigio EH, Siddique T. 2011. Detection of protein aggregation in neurodegenerative diseases. Methods Mol Biol. 793:259-272. doi: 10.1007/978-1-61779-328-8_17. PMID: 21913106.

Drannik A, Martin J, Peterson R, Ma X, Jiang F, Turnbull J. 2017. Cerebrospinal fluid from patients with amyotrophic lateral sclerosis inhibits sonic hedgehog function. PLoS One. 12:e0171668. doi: 10.1371/journal.pone.0171668. PMID: 28170441; PMCID: PMC5295673.

Dyer SC, Austine-Orimoloye O, Azov AG, Barba M, Barnes I, Barrera-Enriquez VP, Becker A, Bennett R, Beracochea M, Berry A, et al. 2025. Ensembl 2025. Nucleic Acids Res. 53:D948-D957. doi: 10.1093/nar/gkae1071. PMID: 39656687; PMCID: PMC11701638.

Elden AC, Kim HJ, Hart MP, Chen-Plotkin AS, Johnson BS, Fang X, Armakola M, Geser F, Greene R, Lu MM, et al. 2010. Ataxin-2 intermediate-length polyglutamine expansions are associated with increased risk for ALS. Nature. 466:1069-1075. doi: 10.1038/nature09320. PMID: 20740007; PMCID: PMC2965417.

Englund A, Kovanen L, Saarikoski ST, Haukka J, Reunanen A, Aromaa A, Lönnqvist J, Partonen T. 2009. NPAS2 and PER2 are linked to risk factors of the metabolic syndrome. J Circadian Rhythms. 7:5. doi: 10.1186/1740-3391-7-5. PMID: 19470168; PMCID: PMC2697141.

Essawy AE, Abdel-Moneim AM, Gaaboub IA, El-Sayed SA. 2011. Adverse effects of dimethyl disulphide on sciatic nerve of Swiss albino mice. Afr J Biotechnol. 10:11081-11086.

Fernandez HL, Stiles JR, Donoso JA. 1986. Skeletal muscle acetylcholinesterase molecular forms in amyotrophic lateral sclerosis. Muscle Nerve. 9:399-406. doi: 10.1002/mus.880090504. PMID: 3724786.

Foran E, Trotti D. 2009. Glutamate transporters and the excitotoxic path to motor neuron degeneration in amyotrophic lateral sclerosis. Antioxid Redox Signal. 11:1587-1602. doi: 10.1089/ars.2009.2444. PMID: 19413484; PMCID: PMC2842587.

Freibaum BD, Chitta RK, High AA, Taylor JP. 2010. Global analysis of TDP-43 interacting proteins reveals strong association with RNA splicing and translation machinery. J Proteome Res. 9:1104-1120. doi: 10.1021/pr901076y. PMID: 20020773; PMCID: PMC2897173.

Fustin JM, Doi M, Yamaguchi Y, Hida H, Nishimura S, Yoshida M, Isagawa T, Morioka MS, Kakeya H, Manabe I, et al. 2013. RNA-methylation-dependent RNA processing controls the speed of the circadian clock. Cell. 155:793-806. doi: 10.1016/j.cell.2013.10.026. PMID: 24209618.

Gao H, Xu C, Liang J, Ge S, Zhang F, Tuo Y, Shi H, Han A. 2022. Pan-cancer analysis of oncogenic role of Programmed Cell Death 2 Like (PDCD2L) and validation in colorectal cancer. Cancer Cell Int. 22:100. doi: 10.1186/s12935-022-02525-x. PMID: 35216602; PMCID: PMC8881831.

Garcia JA, Zhang D, Estill SJ, Michnoff C, Rutter J, Reick M, Scott K, Diaz-Arrastia R, McKnight SL. 2000. Impaired cued and contextual memory in NPAS2-deficient mice. Science. 288:2226-2230. doi: 10.1126/science.288.5474.2226. PMID: 10864874.

García-García R, Martín-Herrero L, Blanca-Pariente L, Pérez-Cabello J, Roodveldt C. 2021. Immune Signaling Kinases in Amyotrophic Lateral Sclerosis (ALS) and Frontotemporal Dementia (FTD). Int J Mol Sci. 22:13280. doi: 10.3390/ijms222413280. PMID: 34948077; PMCID: PMC8707599.

Ge SX, Jung D, Yao R. 2020. ShinyGO: a graphical gene-set enrichment tool for animals and plants. Bioinformatics. 36:2628-2629. doi: 10.1093/bioinformatics/btz931. PMID: 31882993; PMCID: PMC7178415.

Geiger B, Bershadsky A, Pankov R, Yamada KM. 2001. Transmembrane crosstalk between the extracellular matrix--cytoskeleton crosstalk. Nat Rev Mol Cell Biol. 2:793-805. doi: 10.1038/35099066. PMID: 11715046.

Gerdts J, Brace EJ, Sasaki Y, DiAntonio A, Milbrandt J. 2015. SARM1 activation triggers axon degeneration locally via NAD^+ destruction. Science. 348:453-457. doi: 10.1126/science.1258366. PMID: 25908823; PMCID: PMC4513950.

Giordano G, Sánchez-Pérez AM, Montoliu C, Berezney R, Malyavantham K, Costa LG, Calvete JJ, Felipo V. 2005. Activation of NMDA receptors induces protein kinase A-mediated phosphorylation and degradation of matrin 3. Blocking these effects prevents NMDA-induced neuronal death. J Neurochem. 94:808-818. doi: 10.1111/j.1471-4159.2005.03235.x. PMID: 16000164.

Gizowski C, Zaelzer C, Bourque CW. 2016. Clock-driven vasopressin neurotransmission mediates anticipatory thirst prior to sleep. Nature. 537:685-688. doi: 10.1038/nature19756. PMID: 27680940.

Glass JD, Dewan R, Ding J, Gibbs JR, Dalgard C, Keagle PJ, Shankaracharya, García-Redondo A, Traynor BJ, Chia R, et al. 2022. ATXN2 intermediate expansions in amyotrophic lateral sclerosis. Brain. 145:2671-2676. doi: 10.1093/brain/awac167. PMID: 35521889; PMCID: PMC9890463.

Gordon T, Ly V, Hegedus J, Tyreman N. 2009. Early detection of denervated muscle fibers in hindlimb muscles after sciatic nerve transection in wild type mice and in the G93A mouse model of amyotrophic lateral sclerosis. Neurol Res. 31:28-42. doi: 10.1179/174313208X332977. PMID: 18768111.

Grad LI, Rouleau GA, Ravits J, Cashman NR. 2017. Clinical Spectrum of Amyotrophic Lateral Sclerosis (ALS). Cold Spring Harb Perspect Med. 7:a024117. doi: 10.1101/cshperspect.a024117. PMID: 28003278; PMCID: PMC5538408.

Green CB. 2018. Circadian Posttranscriptional Regulatory Mechanisms in Mammals. Cold Spring Harb Perspect Biol. 10:a030692. doi: 10.1101/cshperspect.a030692. PMID: 28778869; PMCID: PMC5983185.

Groen EJ, Fumoto K, Blokhuis AM, Engelen-Lee J, Zhou Y, van den Heuvel DM, Koppers M, van Diggelen F, van Heest J, Demmers JA, et al. 2013. ALS-associated mutations in FUS disrupt the axonal distribution and function of SMN. Hum Mol Genet. 22:3690-3704. doi: 10.1093/hmg/ddt222. PMID: 23681068.

Hirokawa N, Noda Y, Tanaka Y, Niwa S. 2009. Kinesin superfamily motor proteins and intracellular transport. Nat Rev Mol Cell Biol. 10:682-696. doi: 10.1038/nrm2774. PMID: 19773780.

Hughes ME, Hogenesch JB, Kornacker K. 2010. JTK_CYCLE: an efficient nonparametric algorithm for detecting rhythmic components in genome-scale data sets. J Biol Rhythms. 25:372-380. doi: 10.1177/0748730410379711. PMID: 20876817; PMCID: PMC3119870.

Hughes ME, Grant GR, Paquin C, Qian J, Nitabach MN. 2012. Deep sequencing the circadian and diurnal transcriptome of Drosophila brain. Genome Res. 22:1266-1281. doi: 10.1101/gr.128876.111. PMID: 22472103; PMCID: PMC3396368.

Ibrahim F, Maragkakis M, Alexiou P, Maronski MA, Dichter MA, Mourelatos Z. 2013. Identification of in vivo, conserved, TAF15 RNA binding sites reveals the impact of TAF15 on the neuronal transcriptome. Cell Rep. 3:301-308. doi: 10.1016/j.celrep.2013.01.021. PMID: 23416048; PMCID: PMC3594071.

Iradi MCG, Triplett JC, Thomas JD, Davila R, Crown AM, Brown H, Lewis J, Swanson MS, Xu G, Rodriguez-Lebron E, et al. 2018. Characterization of gene regulation and protein interaction networks for Matrin 3 encoding mutations linked to amyotrophic lateral sclerosis and myopathy. Sci Rep. 8:4049. doi: 10.1038/s41598-018-21371-4. PMID: 29511296; PMCID: PMC5840295.

Jobert L, Argentini M, Tora L. 2009. PRMT1 mediated methylation of TAF15 is required for its positive gene regulatory function. Exp Cell Res. 315:1273-1286. doi: 10.1016/j.yexcr.2008.12.008. PMID: 19124016.

Johnson BP, Walisser JA, Liu Y, Shen AL, McDearmon EL, Moran SM, McIntosh BE, Vollrath AL, Schook AC, Takahashi JS, et al. 2014. Hepatocyte circadian clock controls acetaminophen bioactivation through NADPH-cytochrome P450 oxidoreductase. Proc Natl Acad Sci U S A. 111:18757-18762. doi: 10.1073/pnas.1421708111. PMID: 25512522; PMCID: PMC4284582.

Johnson JO, Pioro EP, Boehringer A, Chia R, Feit H, Renton AE, Pliner HA, Abramzon Y, Marangi G, Winborn BJ, et al. 2014. Mutations in the Matrin 3 gene cause familial amyotrophic lateral sclerosis. Nat Neurosci. 17:664-666. doi: 10.1038/nn.3688. PMID: 24686783; PMCID: PMC4000579.

Jung Y, Seo JY, Ryu HG, Kim DY, Lee KH, Kim KT. 2020. BDNF-induced local translation of *GluA1* is regulated by HNRNP A2/B1. Sci Adv. 6:eabd2163. doi: 10.1126/sciadv.abd2163. PMID: 33219033; PMCID: PMC7679154.

Kapeli K, Martinez FJ, Yeo GW. 2017. Genetic mutations in RNA-binding proteins and their roles in ALS. Hum Genet. 136:1193-1214. doi: 10.1007/s00439-017-1830-7. PMID: 28762175; PMCID: PMC5602095.

Khan M, Chen XXL, Dias M, Santos JR, Kour S, You J, van Bruggen R, Youssef MMM, Wan YW, Liu Z, et al. 2024. MATR3 pathogenic variants differentially impair its cryptic splicing repression function. FEBS Lett. 598:415-436. doi: 10.1002/1873-3468.14806. PMID: 38320753.

Kiebler MA, Bassell GJ. 2006. Neuronal RNA granules: movers and makers. Neuron. 51:685-690. doi: 10.1016/j.neuron.2006.08.021. PMID: 16982415.

Klim JR, Williams LA, Limone F, Guerra San Juan I, Davis-Dusenbery BN, Mordes DA, Burberry A, Steinbaugh MJ, Gamage KK, Kirchner R, et al. 2019. ALS-implicated protein TDP-43 sustains levels of STMN2, a mediator of motor neuron growth and repair. Nat Neurosci. 22:167-179. doi: 10.1038/s41593-018-0300-4. PMID: 30643292; PMCID: PMC7153761.

Koike N, Yoo SH, Huang HC, Kumar V, Lee C, Kim TK, Takahashi JS. 2012. Transcriptional architecture and chromatin landscape of the core circadian clock in mammals. Science. 338:349-354. doi: 10.1126/science.1226339. PMID: 22936566; PMCID: PMC3694775.

Kojima S, Shingle DL, Green CB. 2011. Post-transcriptional control of circadian rhythms. J Cell Sci. 124:311-320. doi: 10.1242/jcs.065771. PMID: 21242310; PMCID: PMC3021995.

Kojima S, Sher-Chen EL, Green CB. 2012. Circadian control of mRNA polyadenylation dynamics regulates rhythmic protein expression. Genes Dev. 26:2724-2736. doi: 10.1101/gad.208306.112. PMID: 23249735; PMCID: PMC3533077.

Kondratov RV, Kondratova AA, Gorbacheva VY, Vykhovanets OV, Antoch MP. 2006. Early aging and age-related pathologies in mice deficient in BMAL1, the core componentof the circadian clock. Genes Dev. 20:1868-1873. doi: 10.1101/gad.1432206. PMID: 16847346; PMCID: PMC1522083.

Krach F, Batra R, Wheeler EC, Vu AQ, Wang R, Hutt K, Rabin SJ, Baughn MW, Libby RT, Diaz-Garcia S, et al. 2018. Transcriptome-pathology correlation identifies interplay between TDP-43 and the expression of its kinase CK1E in sporadic ALS. Acta Neuropathol. 136:405-423. doi: 10.1007/s00401-018-1870-7. PMID: 29881994; PMCID: PMC6215775.

Lagier-Tourenne C, Polymenidou M, Hutt KR, Vu AQ, Baughn M, Huelga SC, Clutario KM, Ling SC, Liang TY, Mazur C, et al. 2012. Divergent roles of ALS-linked proteins FUS/TLS and TDP-43 intersect in processing long pre-mRNAs. Nat Neurosci. 15:1488-1497. doi: 10.1038/nn.3230. PMID: 23023293; PMCID: PMC3586380.

Le Gall L, Anakor E, Connolly O, Vijayakumar UG, Duddy WJ, Duguez S. 2020. Molecular and Cellular Mechanisms Affected in ALS. J Pers Med. 10:101. doi: 10.3390/jpm10030101. PMID: 32854276; PMCID: PMC7564998.

Lee JK, Shin JH, Lee JE, Choi EJ. 2015. Role of autophagy in the pathogenesis of amyotrophic lateral sclerosis. Biochim Biophys Acta. 1852:2517-2524. doi: 10.1016/j.bbadis.2015.08.005. PMID: 26264610.

Lehtinen L, Vainio P, Wikman H, Huhtala H, Mueller V, Kallioniemi A, Pantel K, Kronqvist P, Kallioniemi O, Carpèn O, et al. 2017. *PLA2G7* associates with hormone receptor negativity in clinical breast cancer samples and regulates epithelial-mesenchymal transition in cultured breast cancer cells. J Pathol Clin Res. 3:123-138. doi: 10.1002/cjp2.69. PMID: 28451461; PMCID: PMC5402179.

Lin J, Huang P, Chen W, Ye C, Su H, Yao X. 2020. Key Molecules and Pathways Underlying Sporadic Amyotrophic Lateral Sclerosis: Integrated Analysis on Gene Expression Profiles of Motor Neurons. Front Genet. 11:578143. doi: 10.3389/fgene.2020.578143. PMID: 33240324; PMCID: PMC7680998.

Lin Y, Protter DS, Rosen MK, Parker R. 2015. Formation and Maturation of Phase-Separated Liquid Droplets by RNA-Binding Proteins. Mol Cell. 60:208-219. doi: 10.1016/j.molcel.2015.08.018. PMID: 26412307; PMCID: PMC4609299.

Lin YH, Zhen YY, Chien KY, Lee IC, Lin WC, Chen MY, Pai LM. 2017. LIMCH1 regulates nonmuscle myosin-II activity and suppresses cell migration. Mol Biol Cell. 28:1054-1065. doi: 10.1091/mbc.E15-04-0218. PMID: 28228547; PMCID: PMC5391182.

López-Erauskin J, Bravo-Hernandez M, Presa M, Baughn MW, Melamed Z, Beccari MS, Agra de Almeida Quadros AR, Arnold-Garcia O, Zuberi A, Ling K, et al. 2024. Stathmin-2 loss leads to neurofilament-dependent axonal collapse driving motor and sensory denervation. Nat Neurosci. 27:34-47. doi: 10.1038/s41593-023-01496-0. PMID: 37996528; PMCID: PMC10842032.

Lowrey PL, Takahashi JS. 2004. Mammalian circadian biology: elucidating genome-wide levels of temporal organization. Annu Rev Genomics Hum Genet. 5:407-441. doi: 10.1146/annurev.genom.5.061903.175925. PMID: 15485355; PMCID: PMC3770722.

Maday S, Twelvetrees AE, Moughamian AJ, Holzbaur EL. 2014. Axonal transport: cargo-specific mechanisms of motility and regulation. Neuron. 84:292-309. doi: 10.1016/j.neuron.2014.10.019. PMID: 25374356; PMCID: PMC4269290.

Marcheva B, Perelis M, Weidemann BJ, Taguchi A, Lin H, Omura C, Kobayashi Y, Newman MV, Wyatt EJ, McNally EM, et al. 2020. A role for alternative splicing in circadian control of exocytosis and glucose homeostasis. Genes Dev. 34:1089-1105. doi: 10.1101/gad.338178.120. PMID: 32616519; PMCID: PMC7397853. Erratum in: Genes Dev. 2021. 35:425. doi: 10.1101/gad.348303.121. PMID: 32616519; PMCID: PMC7397853.

Martinez FJ, Pratt GA, Van Nostrand EL, Batra R, Huelga SC, Kapeli K, Freese P, Chun SJ, Ling K, Gelboin-Burkhart C, et al. 2016. Protein-RNA Networks Regulated by Normal and ALS-Associated Mutant HNRNPA2B1 in the Nervous System. Neuron. 92:780-795. doi: 10.1016/j.neuron.2016.09.050. PMID: 27773581; PMCID: PMC5123850.

McGlincy NJ, Valomon A, Chesham JE, Maywood ES, Hastings MH, Ule J. 2012. Regulation of alternative splicing by the circadian clock and food related cues. Genome Biol. 13:R54. doi: 10.1186/gb-2012-13-6-r54. PMID: 22721557; PMCID: PMC3446320.

McMillan M, Gomez N, Hsieh C, Bekier M, Li X, Miguez R, Tank EMH, Barmada SJ. 2023. RNA methylation influences TDP43 binding and disease pathogenesis in models of amyotrophic lateral sclerosis and frontotemporal dementia. Mol Cell. 83:219-236.e7. doi: 10.1016/j.molcel.2022.12.019. PMID: 36634675; PMCID: PMC9899051.

Menet JS, Rodriguez J, Abruzzi KC, Rosbash M. 2012. Nascent-Seq reveals novel features of mouse circadian transcriptional regulation. Elife. 1:e00011. doi: 10.7554/eLife.00011. PMID: 23150795; PMCID: PMC3492862.

Milioto C, Carcolé M, Giblin A, Coneys R, Attrebi O, Ahmed M, Harris SS, Lee BI, Yang M, Ellingford RA, et al. 2024. PolyGR and polyPR knock-in mice reveal a conserved neuroprotective extracellular matrix signature in C9orf72 ALS/FTD neurons. Nat Neurosci. 27:643-655. doi: 10.1038/s41593-024-01589-4. PMID: 38424324; PMCID: PMC11001582.

Mojsilovic-Petrovic J, Nedelsky N, Boccitto M, Mano I, Georgiades SN, Zhou W, Liu Y, Neve RL, Taylor JP, Driscoll M, et al. 2009. FOXO3a is broadly neuroprotective in vitro and in vivo against insults implicated in motor neuron diseases. J Neurosci. 29:8236-8247. doi: 10.1523/JNEUROSCI.1805-09.2009. PMID: 19553463; PMCID: PMC2748231.

Moloney EB, de Winter F, Verhaagen J. 2014. ALS as a distal axonopathy: molecular mechanisms affecting neuromuscular junction stability in the presymptomatic stages of the disease. Front Neurosci. 8:252. doi: 10.3389/fnins.2014.00252. PMID: 25177267; PMCID: PMC4132373.

Murakami T, Qamar S, Lin JQ, Schierle GS, Rees E, Miyashita A, Costa AR, Dodd RB, Chan FT, Michel CH, et al. 2015. ALS/FTD Mutation-Induced Phase Transition of FUS Liquid Droplets and Reversible Hydrogels into Irreversible Hydrogels Impairs RNP Granule Function. Neuron. 88:678-690. doi: 10.1016/j.neuron.2015.10.030. PMID: 26526393; PMCID: PMC4660210.

Muzio L, Sirtori R, Gornati D, Eleuteri S, Fossaghi A, Brancaccio D, Manzoni L, Ottoboni L, Feo L, Quattrini A, et al. 2020. Retromer stabilization results in neuroprotection in a model of Amyotrophic Lateral Sclerosis. Nat Commun. 11:3848. doi: 10.1038/s41467-020-17524-7. PMID: 32737286; PMCID: PMC7395176.

Nagano S, Araki T. 2021. Axonal Transport and Local Translation of mRNA in Neurodegenerative Diseases. Front Mol Neurosci. 14:697973. doi: 10.3389/fnmol.2021.697973. PMID: 34194300; PMCID: PMC8236635.

Nagoshi N, Nakashima H, Fehlings MG. 2015. Riluzole as a neuroprotective drug for spinal cord injury: from bench to bedside. Molecules. 20:7775-7789. doi: 10.3390/molecules20057775. PMID: 25939067; PMCID: PMC6272473.

Nakaya T, Alexiou P, Maragkakis M, Chang A, Mourelatos Z. 2013. FUS regulates genes coding for RNA-binding proteins in neurons by binding to their highly conserved introns. RNA. 19:498-509. doi: 10.1261/rna.037804.112. PMID: 23389473; PMCID: PMC3677260.

Nikolaou N, Gordon PM, Hamid F, Taylor R, Lloyd-Jones J, Makeyev EV, Houart C. 2022. Cytoplasmic pool of U1 spliceosome protein SNRNP70 shapes the axonal transcriptome and regulates motor connectivity. Curr Biol. 32:5099-5115.e8. doi: 10.1016/j.cub.2022.10.048. PMID: 36384140.

Nussbacher JK, Tabet R, Yeo GW, Lagier-Tourenne C. 2019. Disruption of RNA Metabolism in Neurological Diseases and Emerging Therapeutic Interventions. Neuron. 102:294-320. doi: 10.1016/j.neuron.2019.03.014. PMID: 30998900; PMCID: PMC6545120.

Pan Q, Shai O, Lee LJ, Frey BJ, Blencowe BJ. 2008. Deep surveying of alternative splicing complexity in the human transcriptome by high-throughput sequencing. Nat Genet. 40:1413-5. doi: 10.1038/ng.259. Erratum in: Nat Genet. 2009. 41:762. PMID: 18978789.

Panda S, Antoch MP, Miller BH, Su AI, Schook AB, Straume M, Schultz PG, Kay SA, Takahashi JS, Hogenesch JB. 2002. Coordinated transcription of key pathways in the mouse by the circadian clock. Cell. 109:307-320. doi: 10.1016/s0092-8674(02)00722-5. PMID: 12015981.

Pantelidou M, Zographos SE, Lederer CW, Kyriakides T, Pfaffl MW, Santama N. 2007. Differential expression of molecular motors in the motor cortex of sporadic ALS. Neurobiol Dis. 26:577-589. doi: 10.1016/j.nbd.2007.02.005. PMID: 17418584.

Patel A, Lee HO, Jawerth L, Maharana S, Jahnel M, Hein MY, Stoynov S, Mahamid J, Saha S, Franzmann TM, et al. 2015. A Liquid-to-Solid Phase Transition of the ALS Protein FUS Accelerated by Disease Mutation. Cell. 162:1066-1077. doi: 10.1016/j.cell.2015.07.047. PMID: 26317470.

Penna MS, Hu RC, Rodney GG, Cooper TA. 2023. The role of *Limch1* alternative splicing in skeletal muscle function. Life Sci Alliance. 6:e202201868. doi: 10.26508/lsa.202201868. PMID: 36977593; PMCID: PMC10052820.

Pizarro A, Hayer K, Lahens NF, Hogenesch JB. 2013. CircaDB: a database of mammalian circadian gene expression profiles. Nucleic Acids Res. 41:D1009-1013. doi: 10.1093/nar/gks1161. PMID: 23180795; PMCID: PMC3531170.

Prashad S, Gopal PP. 2021. RNA-binding proteins in neurological development and disease. RNA Biol. 18:972-987. doi: 10.1080/15476286.2020.1809186. PMID: 32865115; PMCID: PMC8216196.

Qiu H, Lee S, Shang Y, Wang WY, Au KF, Kamiya S, Barmada SJ, Finkbeiner S, Lui H, Carlton CE, et al. 2014. ALS-associated mutation FUS-R521C causes DNA damage and RNA splicing defects. J Clin Invest. 124:981-999. doi: 10.1172/JCI72723. Erratum in: J Clin Invest. 2021. 131:149564. doi: 10.1172/JCI149564. PMID: 24509083; PMCID: PMC3938263.

Rabin SJ, Kim JM, Baughn M, Libby RT, Kim YJ, Fan Y, Libby RT, La Spada A, Stone B, Ravits J. 2010. Sporadic ALS has compartment-specific aberrant exon splicing and altered cell-matrix adhesion biology. Hum Mol Genet. 19:313-328. doi: 10.1093/hmg/ddp498. PMID: 19864493; PMCID: PMC2796893.

Rossi J, Balthasar N, Olson D, Scott M, Berglund E, Lee CE, Choi MJ, Lauzon D, Lowell BB, Elmquist JK. 2011. Melanocortin-4 receptors expressed by cholinergic neurons regulate energy balance and glucose homeostasis. Cell Metab. 13:195-204. doi: 10.1016/j.cmet.2011.01.010. PMID: 21284986; PMCID: PMC3033043.

Rotundo RL. 2003. Expression and localization of acetylcholinesterase at the neuromuscular junction. J Neurocytol. 32:743-766. doi: 10.1023/B:NEUR.0000020621.58197.d4. PMID: 15034265.

Rudic RD, McNamara P, Curtis AM, Boston RC, Panda S, Hogenesch JB, Fitzgerald GA. 2004. BMAL1 and CLOCK, two essential components of the circadian clock, are involved in glucose homeostasis. PLoS Biol. 2:e377. doi: 10.1371/journal.pbio.0020377. PMID: 15523558; PMCID: PMC524471.

Salton M, Elkon R, Borodina T, Davydov A, Yaspo ML, Halperin E, Shiloh Y. 2011. Matrin 3 binds and stabilizes mRNA. PLoS One. 6:e23882. doi: 10.1371/journal.pone.0023882. PMID: 21858232; PMCID: PMC3157474.

Sanchez SE, Petrillo E, Beckwith EJ, Zhang X, Rugnone ML, Hernando CE, Cuevas JC, Herz MAG, Depetris-Chauvin A, Simpson CG, et al. 2010. A methyl transferase links the circadian clock to the regulation of alternative splicing. Nature. 468:112-116. doi: 10.1038/nature09470. PMID: 20962777.

Sanz E, Yang L, Su T, Morris DR, McKnight GS, Amieux PS. 2009. Cell-type-specific isolation of ribosome-associated mRNA from complex tissues. Proc Natl Acad Sci U S A. 106:13939-13944. doi: 10.1073/pnas.0907143106. PMID: 19666516; PMCID: PMC2728999.

Schmidt HB, Rohatgi R. 2016. In Vivo Formation of Vacuolated Multi-phase Compartments Lacking Membranes. Cell Rep. 16:1228-1236. doi: 10.1016/j.celrep.2016.06.088. PMID: 27452472; PMCID: PMC4972689.

Shannon P, Markiel A, Ozier O, Baliga NS, Wang JT, Ramage D, Amin N, Schwikowski B, Ideker T. 2003. Cytoscape: a software environment for integrated models of biomolecular interaction networks. Genome Res. 13:2498-2504. doi: 10.1101/gr.1239303. PMID: 14597658; PMCID: PMC403769.

Shen S, Park JW, Lu ZX, Lin L, Henry MD, Wu YN, Zhou Q, Xing Y. 2014. rMATS: robust and flexible detection of differential alternative splicing from replicate RNA-Seq data. Proc Natl Acad Sci U S A. 111:E5593-601. doi: 10.1073/pnas.1419161111. PMID: 25480548; PMCID: PMC4280593.

Shinohara K, Funabashi T, Nakamura TJ, Mitsushima D, Kimura F. 2002. Differential regulation of pituitary adenylate cyclase-activating peptide receptor variants in the rat suprachiasmatic nucleus. Neuroscience. 110:301-308. doi: 10.1016/s0306-4522(01)00479-1. PMID: 11958871.

Song L, Liu H, Yang W, Yin H, Wang J, Guo M, Yang Z. 2024. Biological functions of the m6A reader YTHDF2 and its role in central nervous system disorders. Biochem Pharmacol. 230:116576. doi: 10.1016/j.bcp.2024.116576. PMID: 39424201.

Tada M, Doi H, Koyano S, Kubota S, Fukai R, Hashiguchi S, Hayashi N, Kawamoto Y, Kunii M, Tanaka K, et al. 2018. Matrin 3 Is a Component of Neuronal Cytoplasmic Inclusions of Motor Neurons in Sporadic Amyotrophic Lateral Sclerosis. Am J Pathol. 188:507-514. doi: 10.1016/j.ajpath.2017.10.007. PMID: 29128563.

Takahashi JS, Hong HK, Ko CH, McDearmon EL. 2008. The genetics of mammalian circadian order and disorder: implications for physiology and disease. Nat Rev Genet. 9:764-75. doi: 10.1038/nrg2430. PMID: 18802415; PMCID: PMC3758473.

Tsunematsu T, Yamauchi E, Shibata H, Maki M, Ohta T, Konishi H. 2010. Distinct functions of human MVB12A and MVB12B in the ESCRT-I dependent on their posttranslational modifications. Biochem Biophys Res Commun. 399:232-237. doi: 10.1016/j.bbrc.2010.07.060. Erratum in: Biochem Biophys Res Commun. 2011. 406:158-159. PMID: 20654576.

Uemura Y, Oshima T, Yamamoto M, Reyes CJ, Costa Cruz PH, Shibuya T, Kawahara Y. 2017. Matrin3 binds directly to intronic pyrimidine-rich sequences and controls alternative splicing. Genes Cells. 22:785-798. doi: 10.1111/gtc.12512. PMID: 28695676.

Ule J, Blencowe BJ. 2019. Alternative Splicing Regulatory Networks: Functions, Mechanisms, and Evolution. Mol Cell. 76:329-345. doi: 10.1016/j.molcel.2019.09.017.

Van Den Bosch L, Van Damme P, Bogaert E, Robberecht W. 2006. The role of excitotoxicity in the pathogenesis of amyotrophic lateral sclerosis. Biochim Biophys Acta. 1762:1068-1082. doi: 10.1016/j.bbadis.2006.05.002. PMID: 16806844.

Vieira de Sá R, Sudria-Lopez E, Cañizares Luna M, Harschnitz O, van den Heuvel DMA, Kling S, Vonk D, Westeneng HJ, Karst H, Bloemenkamp L, et al. 2024. ATAXIN-2 intermediate-length polyglutamine expansions elicit ALS-associated metabolic and immune phenotypes. Nat Commun. 15:7484. doi: 10.1038/s41467-024-51676-0. PMID: 39209824; PMCID: PMC11362472.

Vollmers C, Gill S, DiTacchio L, Pulivarthy SR, Le HD, Panda S. 2009. Time of feeding and the intrinsic circadian clock drive rhythms in hepatic gene expression. Proc Natl Acad Sci U S A. 106:21453-21458. doi: 10.1073/pnas.0909591106. PMID: 19940241; PMCID: PMC2795502.

Wahl MC, Will CL, Lührmann R. 2009. The spliceosome: design principles of a dynamic RNP machine. Cell. 136:701-718. doi: 10.1016/j.cell.2009.02.009. PMID: 19239890.

Wang J, Ji X, Liu J, Zhang X. 2019. Serine/Threonine Protein Kinase STK16. Int J Mol Sci. 20:1760. doi: 10.3390/ijms20071760. PMID: 30974739; PMCID: PMC6480182.

Wang KS, Smeyers J, Eggan K, Budnik B, Mordes DA. 2025. C9ORF72 poly-PR disrupts expression of ALS/FTD-implicated *STMN2* through SRSF7. Acta Neuropathol Commun. 13:67. doi: 10.1186/s40478-025-01977-2. PMID: 40140908; PMCID: PMC11948778.

Wang Q, Abruzzi KC, Rosbash M, Rio DC. 2018. Striking circadian neuron diversity and cycling of *Drosophila* alternative splicing. Elife 7:e35618. doi: 10.7554/eLife.35618. PMID: 29863472; PMCID: PMC6025963.

Wijegunawardana D, Nayak A, Vishal SS, Venkatesh N, Gopal PP. 2025. Ataxin-2 polyglutamine expansions aberrantly sequester TDP-43 ribonucleoprotein condensates disrupting mRNA transport and local translation in neurons. Dev Cell. 60:253-269. doi: 10.1016/j.devcel.2024.09.023. PMID: 39419034.

Yang Y, Li Y, Sancar A, Oztas O. 2020. The circadian clock shapes the *Arabidopsis* transcriptome by regulating alternative splicing and alternative polyadenylation. J Biol Chem. 295:7608-7619. doi: 10.1074/jbc.RA120.013513. PMID: 32303634; PMCID: PMC7261790.

Yeo G, Holste D, Kreiman G, Burge CB. 2004. Variation in alternative splicing across human tissues. Genome Biol. 5:R74. doi: 10.1186/gb-2004-5-10-r74. PMID: 15461793; PMCID: PMC545594.

Young RA, Hagenbüchle O, Schibler U. 1981. A single mouse alpha-amylase gene specifies two different tissue-specific mRNAs. Cell. 23:451-458. doi: 10.1016/0092-8674(81)90140-9. PMID: 6162570.

Zhao M, Kim JR, van Bruggen R, Park J. 2018. RNA-Binding Proteins in Amyotrophic Lateral Sclerosis. Mol Cells. 41:818-829. doi: 10.14348/molcells.2018.0243. PMID: 30157547; PMCID: PMC6182225.

Zhao Q, Hu ZY, Zhang JP, Jiang JD, Ma YY, Li JR, Peng ZG, Chen JH. 2017. Dual Roles of Two Isoforms of Autophagy-related Gene ATG10 in HCV-Subgenomic replicon Mediated Autophagy Flux and Innate Immunity. Sci Rep. 7:11250. doi: 10.1038/s41598-017-11105-3. PMID: 28900156; PMCID: PMC5595887.

Zhou Y, Zhou B, Pache L, Chang M, Khodabakhshi AH, Tanaseichuk O, Benner C, Chanda SK. 2019. Metascape provides a biologist-oriented resource for the analysis of systems-level datasets. Nat Commun. 10:1523. doi: 10.1038/s41467-019-09234-6. PMID: 30944313; PMCID: PMC6447622.